ornl

OAK RIDGE NATIONAL LABORATORY

MARTIN MARIETTA

ORNL/TM-10903

MARTIN MARIETTA ENERGY SYSTEMS LIBRARIES

3 4456 0284118 3

Theoretical Studies of Hadronic Calorimetry for High Luminosity, High Energy Colliders

James E. Brau
Tony A. Gabriel

OAK RIDGE NATIONAL LABORATORY
CENTRAL RESEARCH LIBRARY
CIRCULATION SECTION
4500N ROOM 175
LIBRARY LOAN COPY
DO NOT TRANSFER TO ANOTHER PERSON
If you wish someone else to see this report, send in name with report and the library will arrange a loan.

OPERATED BY
MARTIN MARIETTA ENERGY SYSTEMS, INC.
FOR THE UNITED STATES
DEPARTMENT OF ENERGY

Printed in the United States of America. Available from
National Technical Information Service
U.S. Department of Commerce
5285 Port Royal Road, Springfield, Virginia 22161
NTIS price codes—Printed Copy: A04; Microfiche A01

This report was prepared as an account of work sponsored by an agency of the United States Government. Neither the United States Government nor any agency thereof, nor any of their employees, makes any warranty, express or implied, or assumes any legal liability or responsibility for the accuracy, completeness, or usefulness of any information, apparatus, product, or process disclosed, or represents that its use would not infringe privately owned rights. Reference herein to any specific commercial product, process, or service by trade name, trademark, manufacturer, or otherwise, does not necessarily constitute or imply its endorsement, recommendation, or favoring by the United States Government or any agency thereof. The views and opinions of authors expressed herein do not necessarily state or reflect those of the United States Government or any agency thereof.

ORNL/TM-10903

Engineering Physics and Mathematics

Theoretical Studies of Hadronic Calorimetry for High Luminosity, High Energy Colliders

James E. Brau*

Tony A. Gabriel

DATE PUBLISHED —JANUARY 1989

*University of Oregon, Eugene, OR 97403
Submitted for publication.

NOTICE: This document contains information of a preliminary nature. It is subject to revision or correction and therefore does not represent a final report.

Prepared by the
OAK RIDGE NATIONAL LABORATORY
Oak Ridge, Tennessee 37831
operated by
MARTIN MARIETTA ENERGY SYSTEMS, INC.
for the
U.S. DEPARTMENT OF ENERGY
under contract DE-AC05-84OR21400

MARTIN MARIETTA ENERGY SYSTEMS LIBRARIES

3 4456 0284118

CONTENTS

ABSTRACT v
1. INTRODUCTION 1
2. FUNDAMENTAL PHYSICS OF COMPENSATING CALORIMETERS . 3
2.1 BASIC IDEAS 3
2.2 BINDING ENERGY LOSSES 6
2.3 NEUTRONS 6
2.4 EARLY CALCULATIONS 11
2.5 HYDROGENOUS MEDIA 16
2.6 ELECTROMAGNETIC SAMPLING 19
3. THE OPTIONS FOR CALORIMETRY AT FUTURE COLLIDERS . . 22
4. CALCULATIONS OF THE RESPONSE OF HADRONIC CALORIMETERS EMPLOYING SILICON DETECTOR READOUT 24
5. CONCLUSIONS 34
6. APPENDIX: THE METHOD OF CALCULATION 35
7. ACKNOWLEDGEMENTS 38
REFERENCES 39

ABSTRACT

Experiments at the high luminosity, high energy colliders of the future are going to demand optimization of the state of the art of calorimetry design and construction. During the past few years, the understanding of the basic phenomenology of hadron calorimeters has advanced through paralleled theoretical and experimental investigations. The important underlying processes are reviewed to set the framework for the presentation of recent calculations of the expected performance of silicon detector based hadron calorimeters. Such devices employing uranium are expected to achieve the compensation condition (that is, $e/h \approx 1.0$) based on the understanding that has been derived from the uranium-liquid argon and uranium-plastic scintillator systems. In fact, even lead-silicon calorimeters are found to achieve the attractive value for the e/h ratio of 1.16 at 10 GeV.

1. INTRODUCTION

The physics results of future high luminosity, high energy colliders (eg. SSC or LHC) will depend on having very good calorimeters, which have been designed and constructed using the latest state of the art techniques. Many reviews have summarized the existing knowledge of calorimeter physics.[1-4] However, the understanding of the fundamental processes which limit calorimeter performance has undergone a significant advancement in recent years. It will be crucial to apply this understanding in the best ways. The present understanding has evolved through an interchange between theoretical calculations and experimental test programs, as the conclusions drawn from the theory in the calculations have been tested and found to be fundamentally sound.

Four years ago a new understanding of the underlying mechanisms of compensating calorimetry was introduced.[5-10] At that time the following critical points were realized:

1. prior to later experimental confirmation, it was pointed out that current designs of uranium liquid argon calorimeters were not fully compensating;[5-9]
2. the importance of the hydrogen content in the active medium to couple the low energy neutrons to the output signal was stressed;[5-9]
3. the significant role of "electromagnetic sampling inefficiencies" (which are the result of preferential photon absorption[11] and electron multiple scattering in the high-Z inactive material[6,9]) in reducing the ratio of electron to hadron response was explained;[5-9]
4. the importance of the saturation of signal in the regions of high density energy deposition was emphasized;[5-9] and
5. these new understandings led us to "predict that a lead calorimeter may also give EM/HAD ≈ 1,"[12] where EM/HAD is the ratio of average electron to hadron response for the same incident kinetic energy, hereafter referred to as the e/h ratio. In other words, a compensating lead calorimeter was predicted.

At the time this new understanding was introduced in 1984, it was not generally accepted and met with much scepticism in the community. As a result of much experimental testing in the past four years, this scepticism has evolved to a general acceptance by the community. Shortly after the new understanding of compensation was announced, the experimental test programs of D0 at Fermilab and SLD at SLAC presented new data which supported the partial compensation expected for uranium liquid argon calorimeters. Table 1 shows the comparison of calculations with results presented at the Caltech Workshop on Compensated Calorimetry in 1985.[9] As is seen, the predictions of the Monte Carlo calculations agreed very well with the new measurements. Furthermore, the interpretation of the fundamental processes driving this behaviour had been determined and was presented at that time. The understanding of the role of hydrogen was expanded with the introduction of a prediction by Brüeckmann[13] of "tuning" of relative electron and hadron response by varying the ratio of uranium plate thickness to the scintillator thickness. Test beam studies of uranium scintillator calorimeters have confirmed the expected trends from the model of "tuning".[14] Considerations of the role of "tuning" in

nonuranium scintillator calorimeters led to a specific design of a lead-scintillator compensating calorimeter with the ratio of lead thickness to scintillator thickness of approximately four; it was subsequently built and found to have e/h = 1.05 ± 0.04.[15] Recently an activation analysis[16] of calorimeter-like stacks at CERN has confirmed the details of neutron-hydrogen coupling[7,8] which were key to the new understanding of calorimetry introduced in 1984. This new understanding has now been generally accepted and serves as the foundation of recent reviews of the phenomenology of compensating calorimeters.[17,18]

Table 1
The comparison of CALOR calculations with SLD and D0 measurements.*

			$\frac{\sigma_\pi}{E_\pi}$		e/π	
			Data	*Monte Carlo*	Data	*Monte Carlo*
11 GeV	Pb/G10	SLD	18.7	21	1.24	1.28
11 GeV	U/Fe/G10	SLD	18.4	19	1.26	1.27
11 GeV	U/Pb	SLD	21.4	20	1.20	1.30
11 GeV	U/U	SLD	18.2	20	1.17	1.22
10 GeV	U	D0	19	18*	1.1	1.14*

*These were presented at the Workshop on Compensated Calorimetry.[9]

The challenge of doing physics at the next generation hadron colliders will be great. Event rates are being planned at the 100 MHz level, meaning that fast calorimeters must be built to minimize pileup. The experience at the Sp$\bar{p}$S of the importance of nearly full event containment (i.e. hermeticity) will be repeated. Many searches for new particles will demand good reconstruction of missing energy, for example the search for additional intermediate bosons such as $W' \rightarrow e\nu$. Excellent energy resolutions with good linearity and gaussian resolution functions are required for many experiments, such as the search for compositeness at the tens of TeV energy scale.[19] The search for such structure in the high-p_T jet signature will test the best calorimeters. While all these performance characteristics are necessary, they must exist in a very hostile radiation environment.[20] Neutron fluxes in excess of 10^{12} cm^{-2} yr^{-1} and doses of greater than 10^3 Grays/year in calorimeters situated at a radius of two meters from the interaction point are anticipated at the next generation of hadron colliders. These requirements of performance and survivability will test the present understanding of calorimeter physics and designers' ingenuity in building radiation hardened equipment. The understanding of all fundamental processes is essential to a successful program.

2. FUNDAMENTAL PHYSICS OF COMPENSATING CALORIMETERS

2.1 BASIC IDEAS

The understanding of compensating calorimeters begins with the appreciation for the original motivation of the inventors of the technique.[21] It must be realized that hadronic cascades which contain large amounts of electromagnetic energy have less losses of energy due to nuclear breakup than those which contain little electromagnetic energy and therefore a large number of hadronic interactions. This comparison is illustrated in Figure 1. Figure 1a illustrates the situation for non-compensating calorimeters. The overall distribution is created by summing a variety of different types of events. The two extremes, here called type A and type B, result in quite different responses. The type A events have a large fraction of the incident hadron energy converted to π^0s and other forms of electromagnetic energy, and therefore there are few hadronic nuclear interactions. Since the π^0s yield an observed signal which is comparable to the response of the calorimeter to incident electrons of the same energy and there is little energy lost to the breakup of nuclei, the e/h ratio for such events is nearly one, as shown in Figure 1a. Type B events in such non-compensating calorimeters, on the other hand, show large amounts of lost energy in the nuclear breakup resulting from the many hadronic nuclear interactions. This includes nuclear binding energy losses, as well as losses from heavy fragment production, neutrino production, and low energy nucleon generation. All of these processes result in a reduction in the detectable energy in the calorimeter. These type B cascades have a minimal amount of generated electromagnetic energy and the resulting e/h ratio is much less than one. Combining all types of hadronic cascades, from type A to type B and everything in between, leads to a very broad distribution of responses, and a resulting poor resolution for the measured energy deposition.

Figure 1b illustrates the situation for compensating calorimeters where the response to events of type A and type B has been equalized by a cleverly designed calorimeter. This is the basis for the original ideas as presented in Ref. 21. It can be seen from the figure that type A events respond with a signal nearly equal to an electron signal. However, the type B events also give an average response that is nearly comparable to the response of an electron. The nuclear breakup energy has been *compensated for*, by designing the calorimeter to preferentially respond to the low energy neutron component of the shower, which is correlated with the lost nuclear breakup energy. As will be shown later, it is not necessary to fully recover all of the nuclear breakup energy as the electromagnetic response is also suppressed in high Z materials due to processes occurring at the very low energy portion of the electromagetic shower. The role of these sampling inefficiencies which result from the preferential photon absorption[11] and the electron multiple scattering in the inactive material[6,9] has a very stong effect on the calorimeter response. A proper balance of the electromagnetic suppression and the preferential sampling of low energy neutrons leads to this equalization of the average response of type A and type B events. As a result, the sum of all the types of events, from A to B, yields a

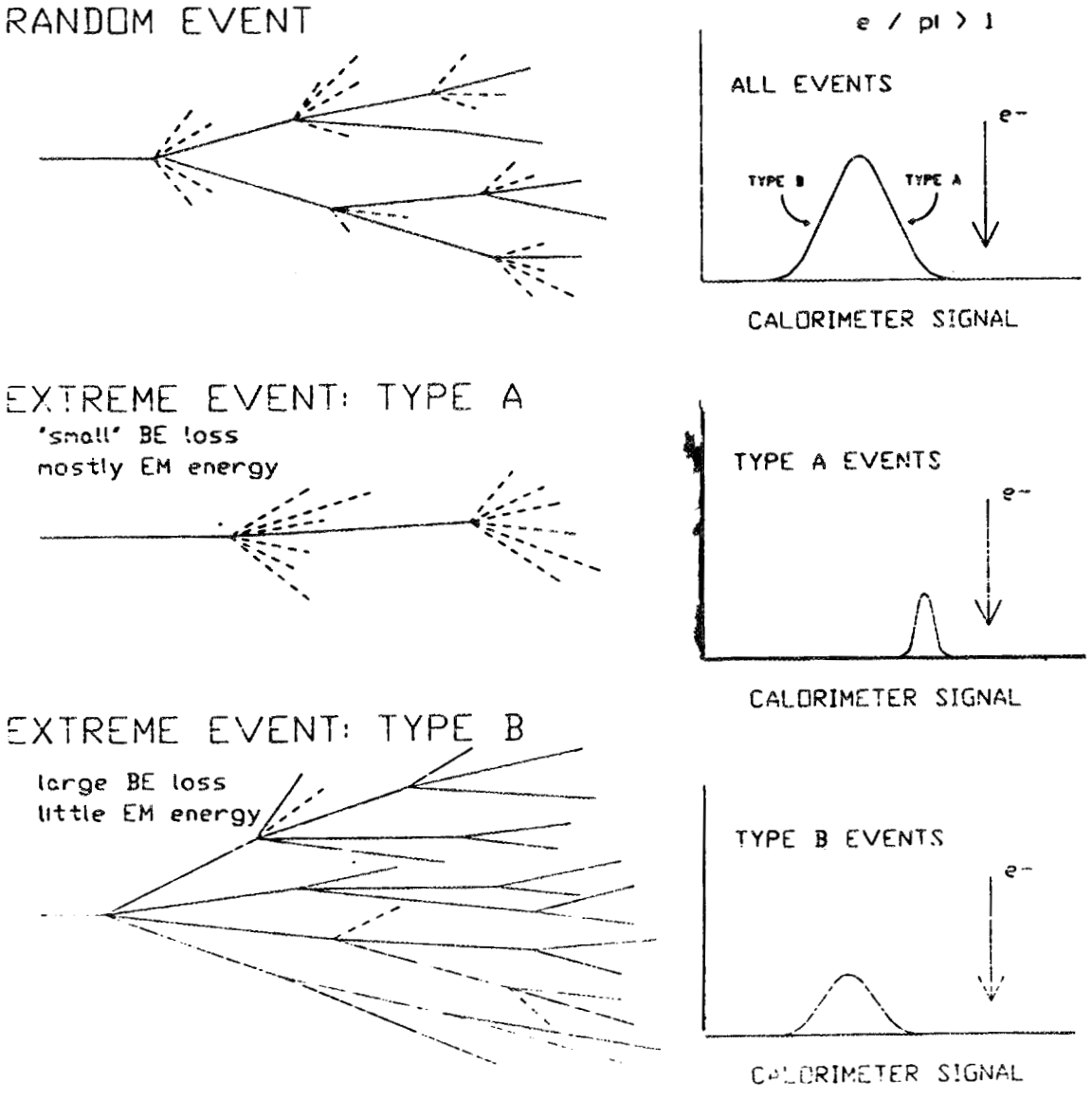

Fig. (1a) An illustration of the origin of e/h > 1 in noncompensating calorimeters.

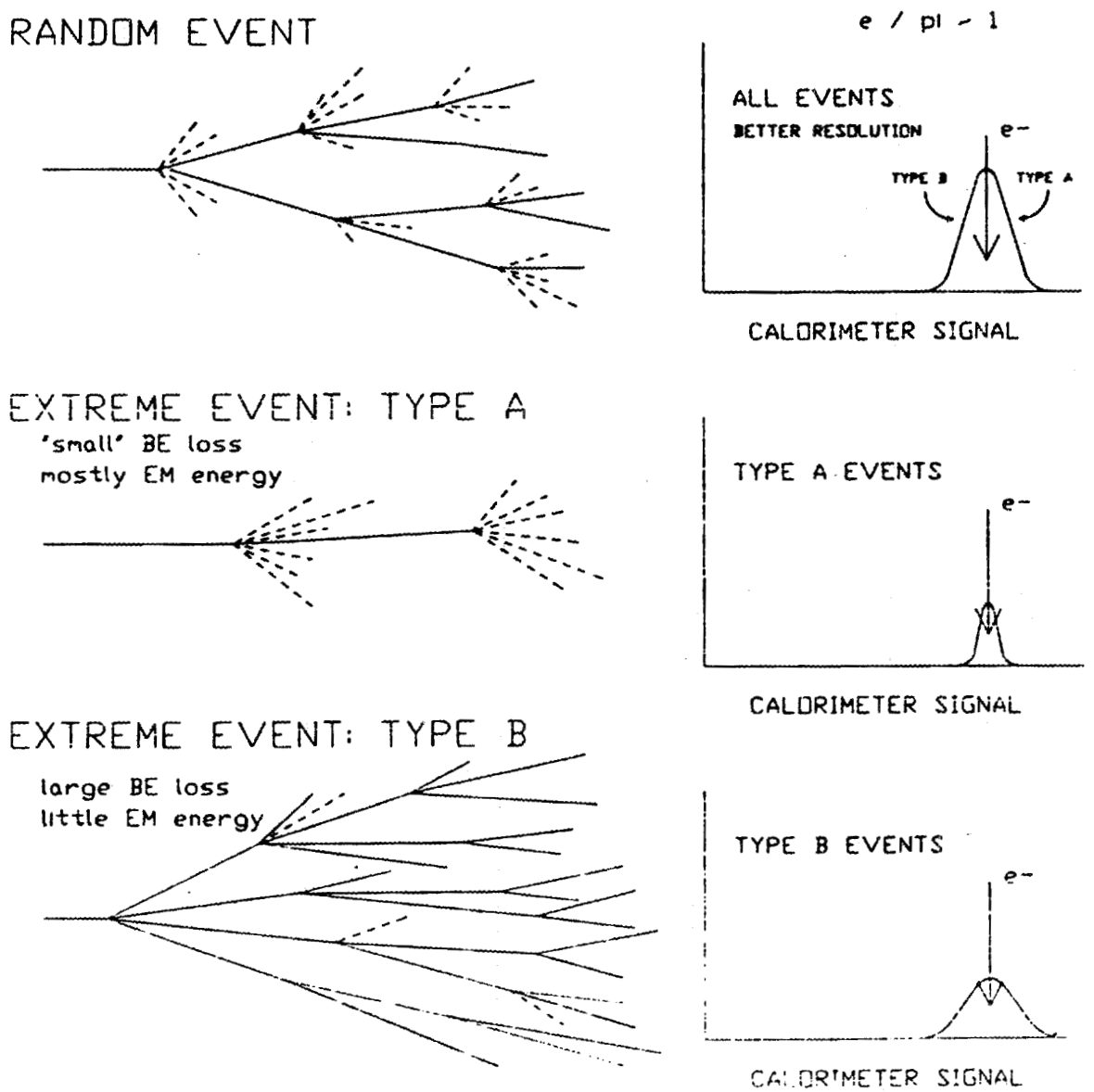

Fig. (1b) An illustration of the origin of e/h $\approx$ 1 in compensating calorimeters. This underlying role of electromagnetic and binding-energy losses to the fluctuations in energy distributions was described in Ref. 21 to motivate the development of compensating calorimeters.

narrower distribution; that is, the energy resolution is greatly improved. This is the motivation for examining the ratio e/h as a measure of the degree of compensation.

2.2 BINDING ENERGY LOSSES

In previous studies of the detailed processes occurring in hadronic cascades, extensive use has been made of the CALOR code system(HETC, EGS, MORSE, MICAP, SPECT, LIGHT, etc. -- see the Appendix for details).[22] Figure 2, for example, presents the calculated distribution from HETC of energy lost through the release of nuclear binding at the first interaction of a 5 GeV π^- in a uranium scintillator sampling calorimeter composed of alternating three millimeter uranium plates and scintillator sheets. An average energy loss of 380 MeV occurs at the first interaction sites. This represents 7.6% of the incident hadron's energy removed from the cascade at the first interaction. For lower energy interactions the loss is naturally going to be smaller, but only somewhat since for the same calorimeter HETC predicts an average loss of 200 MeV at the first interaction of 1 GeV incident neutrons. Notice that this represents twenty percent of the incident hadron kinetic energy. For lighter target materials, such as iron, the value will be somewhat less.[23]

As the shower progresses many additional interactions lead to an accumulated energy loss. Figure 3 shows the distribution of the number of nuclear interactions (excluding elastic collisions) in HETC for the incident 5 GeV π^- on this uranium scintillator stack. There are an average of 24 collisions,[24] while some showers terminate as the pion decays in the stack (notice three of these 500 showers had no nuclear collisions). Integrating the binding energy loss over these many interactions yields the distribution of binding energy lost for the entire showers as shown in Figure 4. On average 32% of the incident kinetic energy is lost in binding energy associated with the ejection of nucleons (primarily low energy) from the nuclei. The 1600 MeV has been lost, but one remaining effect is the large number of low energy neutrons created in the nuclear disruption. Figure 5 shows the correlation of the energy content of the low energy neutrons (kinetic energy below 20 MeV) with the binding energy lost in each of the hadronic cascades. Events with small binding energy losses naturally have disrupted the nuclei to the smallest extent and have transferred the least energy to low energy nucleons. Events with large binding energy losses have resulted from a large number of very disruptive collisons, resulting in large amounts of energy being carried by the low energy nucleons. These trends are very evident in Figure 5. It was this strong correlation which motivated the first attempts at the construction of compensating calorimeters.[21] It was reasoned that by increasing the neutron content through the fission process in the calorimeter, the binding energy losses could be overcome in a fashion which was proportional to the losses, thereby leading to an improved resolution. To achieve this end, uranium was employed as a radiator material.

2.3 NEUTRONS

The key to successfully capitalizing on this correlation is through the coupling of these low energy neutrons to the sampling medium. Eventually, most of these low energy neutrons are captured by ^{238}U, yielding approximately eight MeV per neutron capture in prompt gammas. In addition, prompt fission gammas are produced in the fission process. Unfortunately, the sampling medium is very

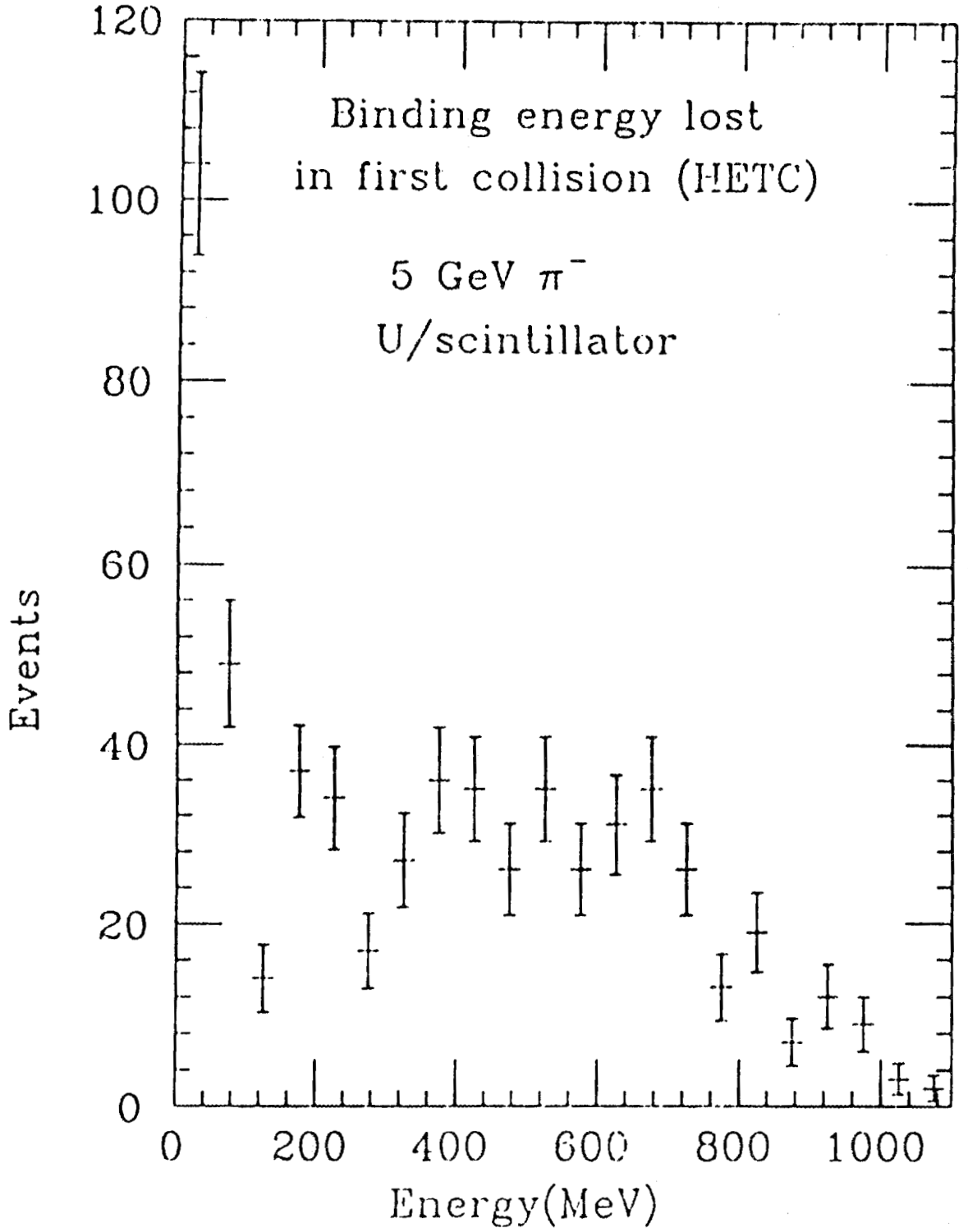

Fig. 2. The distribution of binding energy lost in the first collision of a 5 GeV π^- on a uranium-scintillator calorimeter made of 3 mm uranium plates and 3 mm scintillator sheets as calculated by HETC. The average value is 380 MeV.

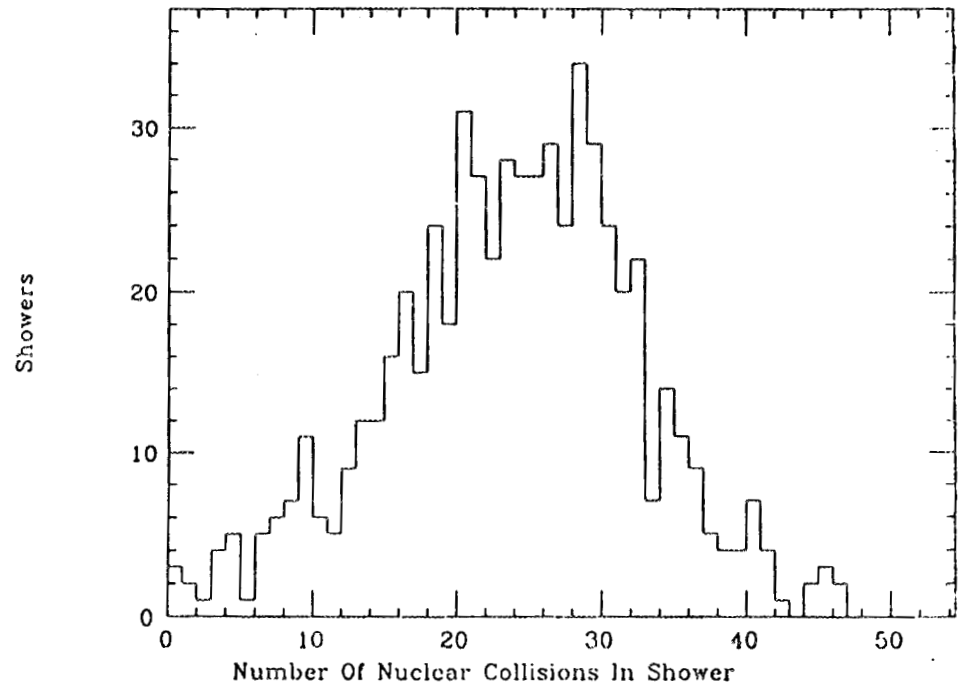

Fig. 3. The distribution of the number of nuclear interations by a 5 GeV π^- on a uranium-scintillator calorimeter made of 3 mm uranium plates and 3 mm scintillator sheets as calculated by HETC. The neutrons in the cascade are cutoff for this count at 20 MeV. The average number of collisions is 24.

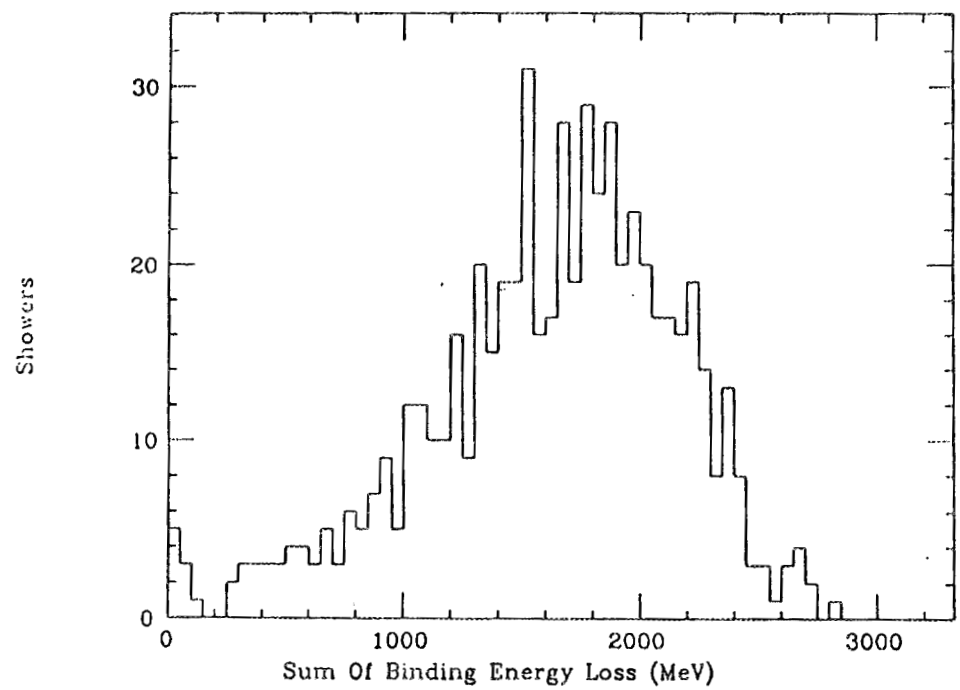

Fig. 4. The distribution of total binding energy losses per shower from a 5 GeV π^- on a uranium-scintillator calorimeter made of 3 mm uranium plates and 3 mm scintillator sheets as calculated by HETC. The average energy lost is 1600 MeV, 32% of the incident particle energy.

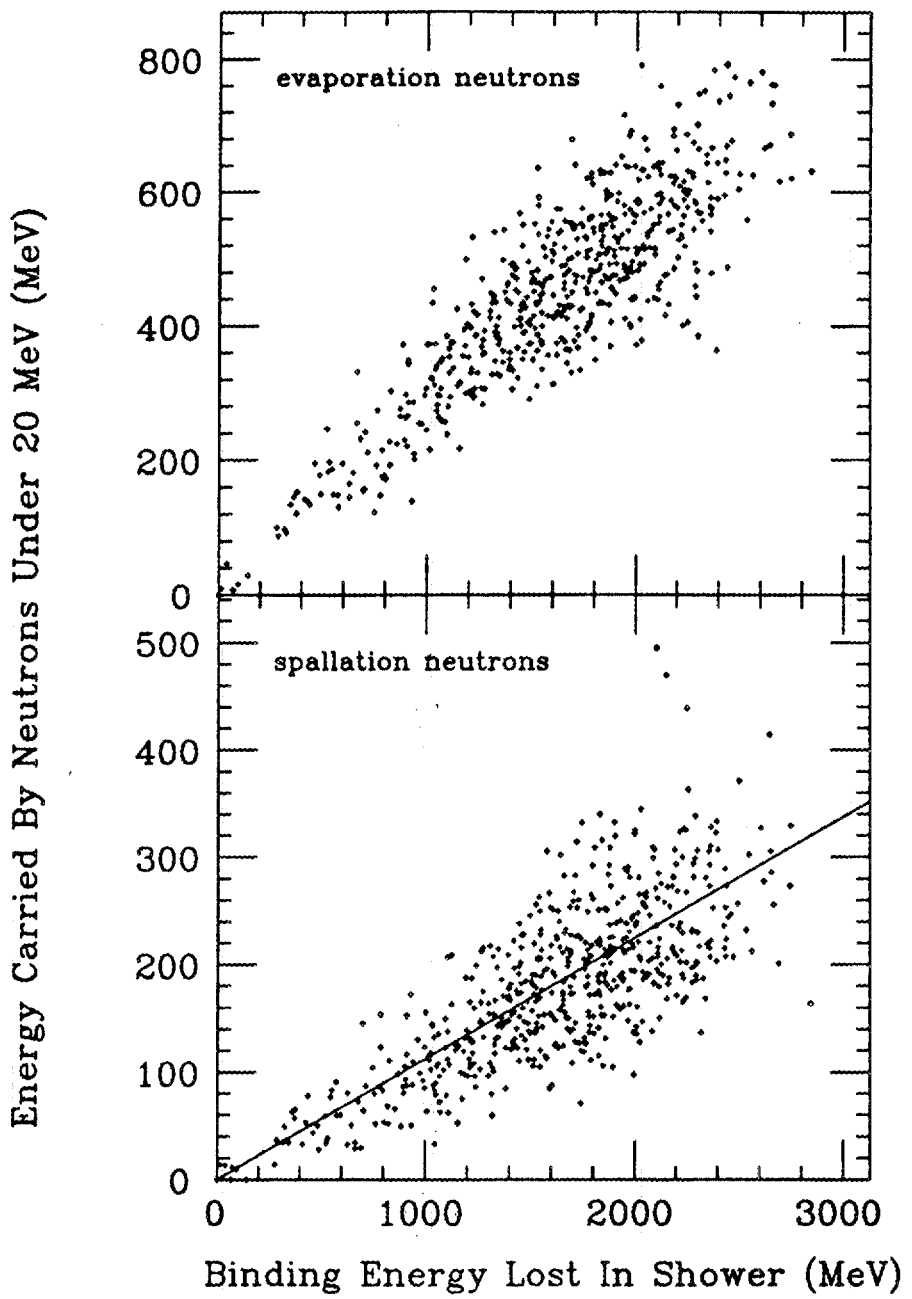

Fig. 5. The correlation of energy carried by neutrons below 20 MeV to the binding energy lost in showers from 5 GeV π^- on a uranium-scintillator calorimeter made of 3 mm uranium plates and 3 mm scintillator sheets as calculated by HETC. The distribution is presented both for the evaporation neutrons and the spallation neutrons. The solid line shows the average trend of the data and is plotted for comparison with Fig. 6.

inefficient to sampling these soft gammas due to the effects described earlier regarding preferential absorption in the high Z material. Also the time scale associated with thermalization of the neutrons is too long ($\sim \mu$ s). Therefore, the signal from the neutrons must come from their direct interaction in the active medium.[25] Figure 6 shows the observed neutron energy which our calculations predict will be sampled by the plastic scintillator in the three millimeter uranium-scintillator stack. This distribution results from detailed calculations which were performed with the Oak Ridge Monte Carlo Codes HETC and MORSE (see the Appendix for details.) The solid line drawn on this figure represents the average energy carried by the spallation neutrons before transport; this is the same line as is shown on Figure 5. Notice that a very large fraction of the original neutron energy (even after the effects of saturation have been taken into account) has been observed ($\sim$ 12%). This is due to neutron amplification by fission of the uranium and the very efficient transfer of neutron energy to the hydrogen, which will be discussed later. For comparison, the fraction of electromagnetic energy observed is about 6%.

Since the transfer is so complete in the hydrogenous plastic scintillator, the relative contribution of the total signal can be varied by changing the relative thickness of the sampling layer and the uranium radiator, as was pointed out first in Ref. 13. This is illustrated in our calculations shown in Figure 7. A calorimeter composed of three millimeter uranium plates and three millimeter plastic scintillator plates gives approximately the correct fraction of neutron coupling to bring the e/h ratio to 1.0. When the radiator thickness is increased to six millimeters, the scintillator thickness must be considerably greater than six millimeters to achieve e/h = 1.0. The neutron energy has been significantly reduced by the first three millimeters of scintillator and therefore the doubling of thickness does not double the neutron coupled energy.

It is important to understand in detail the fission processes which take place in the calorimeter stack. Recent activation analysis measurements[16] have confirmed the basic level of fissions calculated with the CALOR code system.[26] In the early work of Ref. 26, two fission numbers were presented as a basis for studying the cascade process. One was the calculated number of fissions expected for an infinite, natural uranium system with no cutoff in time. Naturally this yields an upper limit of the expected number of fissions. These results are shown in Table 2. For 2 and 5 GeV kinetic energy protons, one finds $\sim$ 24 fissions per GeV. When the stack is restricted to a geometry similar to that of the early test device of Ref. 21 and a time cut of 50 nanoseconds is applied, the number of fissions drops to 6 per GeV. As Table 2 shows, this is consistent with the recent measurements of Ref. 16. Recently, for the Task Force on Radiation in the SSC Interaction Regions, calculations[27] were carried out to determine the numbers of fissions induced by neutrons of kinetic energies below 20 MeV for the two stacks studied experimentally by Ref. 16. These results are presented in Table 2. Reasonable agreement has been obtained for the massive uranium stack case, but the size of the measured number of fissions for the uranium-scintillator case remains a puzzle. One would expect the number to drop by a larger fraction than measured as the coupling of the neutrons to the hydrogen in the plastic scintillator rapidly drops the neutron energies below the fast fission threshold of ^{238}U at approximately 1 MeV.

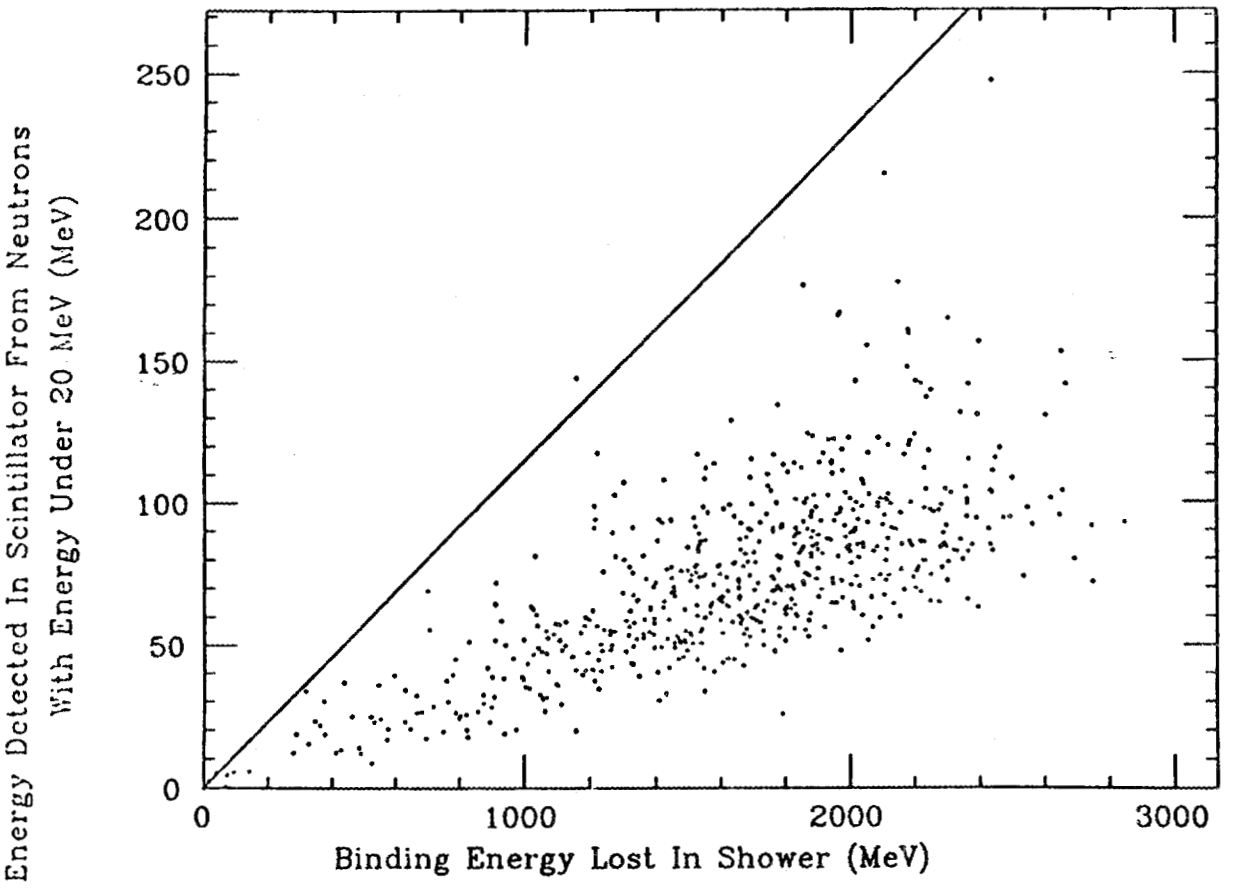

Fig. 6. The correlation of energy detected in the scintillator from the neutrons with energy below 20 MeV to the binding energy lost in showers from 5 GeV π^- on a uranium-scintillator calorimeter made of 3 mm uranium plates and 3 mm scintillator sheets as calculated by HETC and MORSE. The solid line shows the average trend of the data in Fig. 5. Comparison of the solid curve and the trend of the data in this figure shows that the fraction of neutron energy which has been detected is very large. This results from the uranium amplification of the neutron signal and the very efficient transfer of neutron energy to the hydrogen in the scintillator.

Accurate predictions of performance also require a knowledge of the relative time of response for the various components of the calorimeter signal. Figure 8 shows temporal reponse functions for the fission and neutron capture processes expected in an infinite natural uranium system as presented in Ref. 26. The time-dependence of these responses for other uranium calorimeters will be somewhat modified due to the effects of other materials and system sizes, but the basic time-dependence will remain similar. Since the capture energy will be inefficiently transferred to the signal, the majority of the hadronic response of uranium calorimeters occurs in the first 50-100 nanoseconds.

2.4 EARLY CALCULATIONS

All of the effects mentioned above were included in our earlier studies of compensating calorimeters. A review of these earlier calculations is useful to

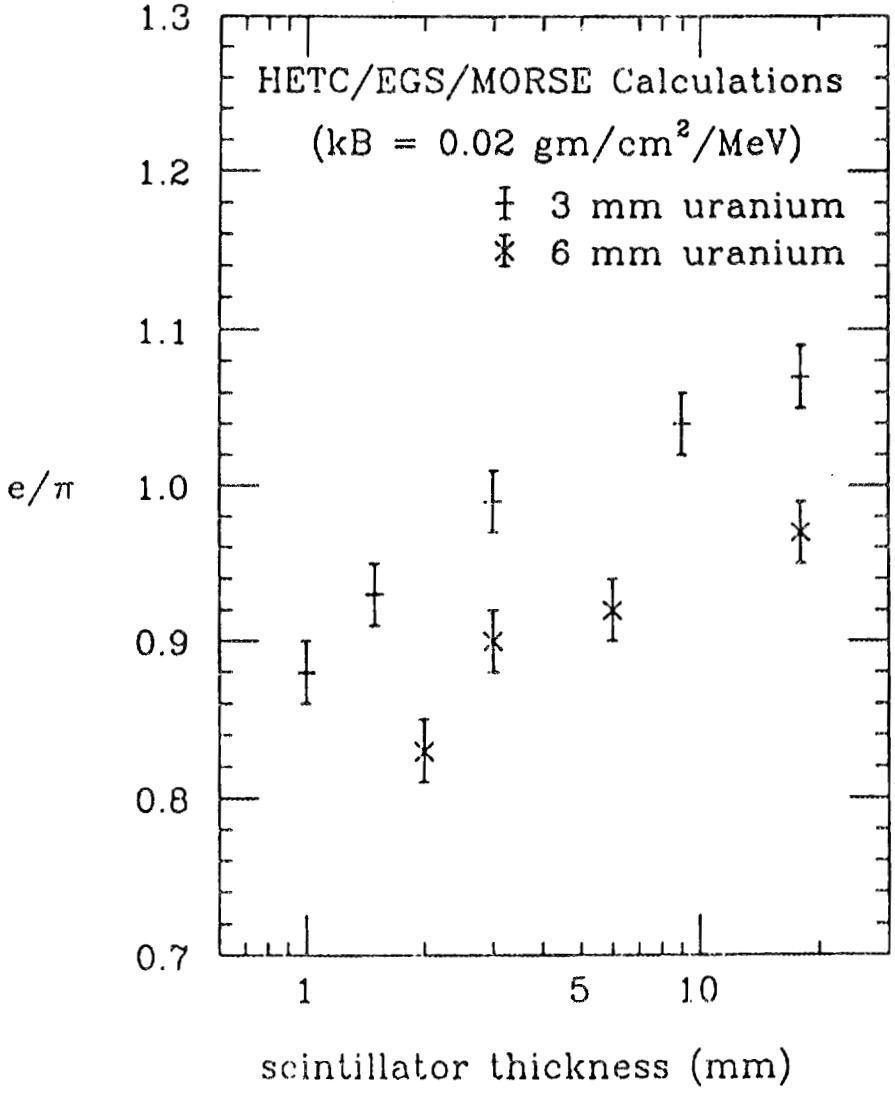

Fig. 7. The variation of e/π with scintillator thickness for a set of uranium-scintillator calorimeter calculations for incident 5 GeV π^-. This figure illustrates the "tuning" possible with scintillator, first noted in Ref. 13.

Table 2
Comparison of calculations of the numbers of fissions with the experimentally deduced values.

	Calculations	Experiment[16]
infinite, massive natural uranium with no time cut (2 & 5 GeV protons)	24/GeV[25]	
U/liquid argon restricted hexagonal calorimeter geometry of Ref. 21 with time cut of 50 nsec (2,5,10,&20 GeV p)	6/GeV[25]	
massive depleted uranium, 20x120 cm^2 with no time cut (591 MeV protons)	5.6±0.3/GeV[26]	6.4±0.7/GeV
U/scintillator 20x120 cm^2 with no time cut (591 MeV protons)	2.4±0.2/GeV[26]	5.1±0.7/GeV

In each case the number of fissions has been normalized per GeV of incident particle energy. The reader is cautioned that the normalization of the data to energy deposition, as presented in Ref. 16, is done differently as those authors "correct" for some ineffective energy losses. Since the normalization is done here in the same way for both data and calculations, the comparison between calculations and experiment is direct.

understand the new results to be presented later. In Fig. 9, the response of a simulation[7] of the AFS calorimeter tests[28] is given. This stack was less than 4 interaction lengths deep, so that a fraction of the energy in the hadronic showers was not fully contained. This leads to the low energy tail on the calculated pulse height distribution and was also apparent on the experimental data. For the set of parameters presented in Fig. 9 an e/h ratio of 1.02 was calculated for the all uranium case. Figure 10 shows comparisons between calculations[7] and AFS measurements[28] for various ratios of iron (copper) and uranium in the calorimeter. Note that for these comparisons, the differences between iron and copper do not alter the basic results and conclusions. As the data and calculations show, the compensation resulting from increasing fractions of uranium radiator is well understood.

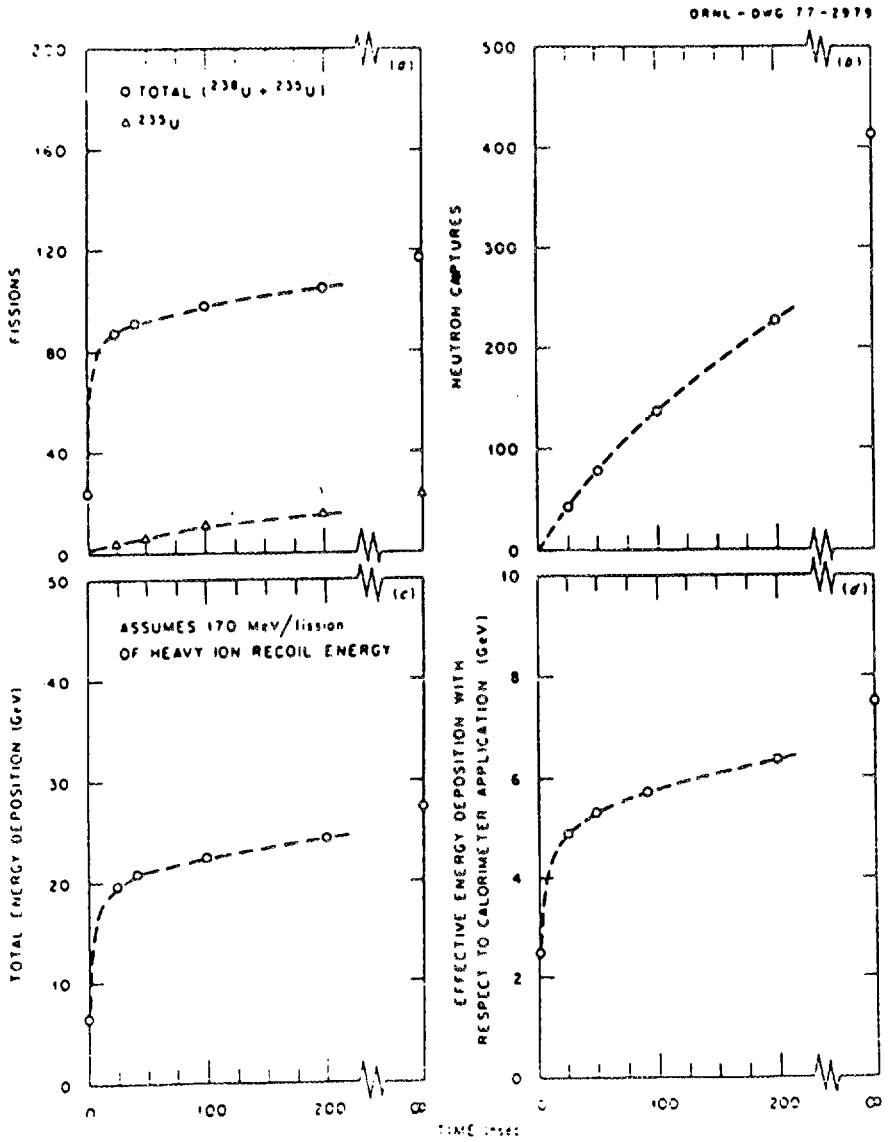

Fig. 8. The temporal dependence of the fissions and neutron captures occurring in an infinite uranium system for incident 5 GeV protons, first presented in Ref. 26.

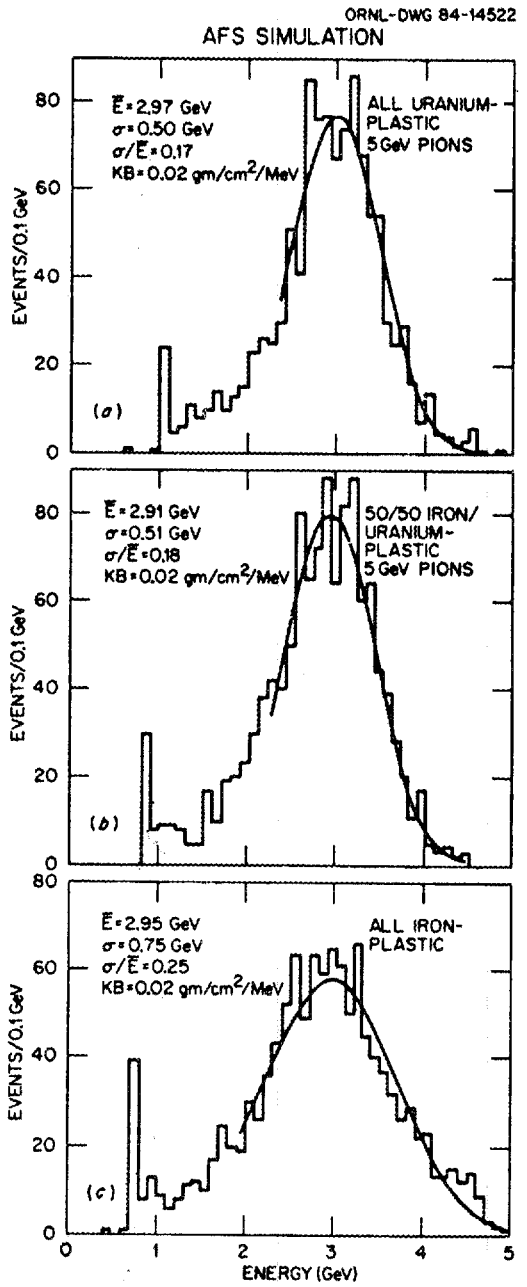

Fig. 9. The calculated pulse height distribution of the uranium-scintillator calorimeter (simulating the AFS Collaboration calorimeter) as presented in Ref. 7.

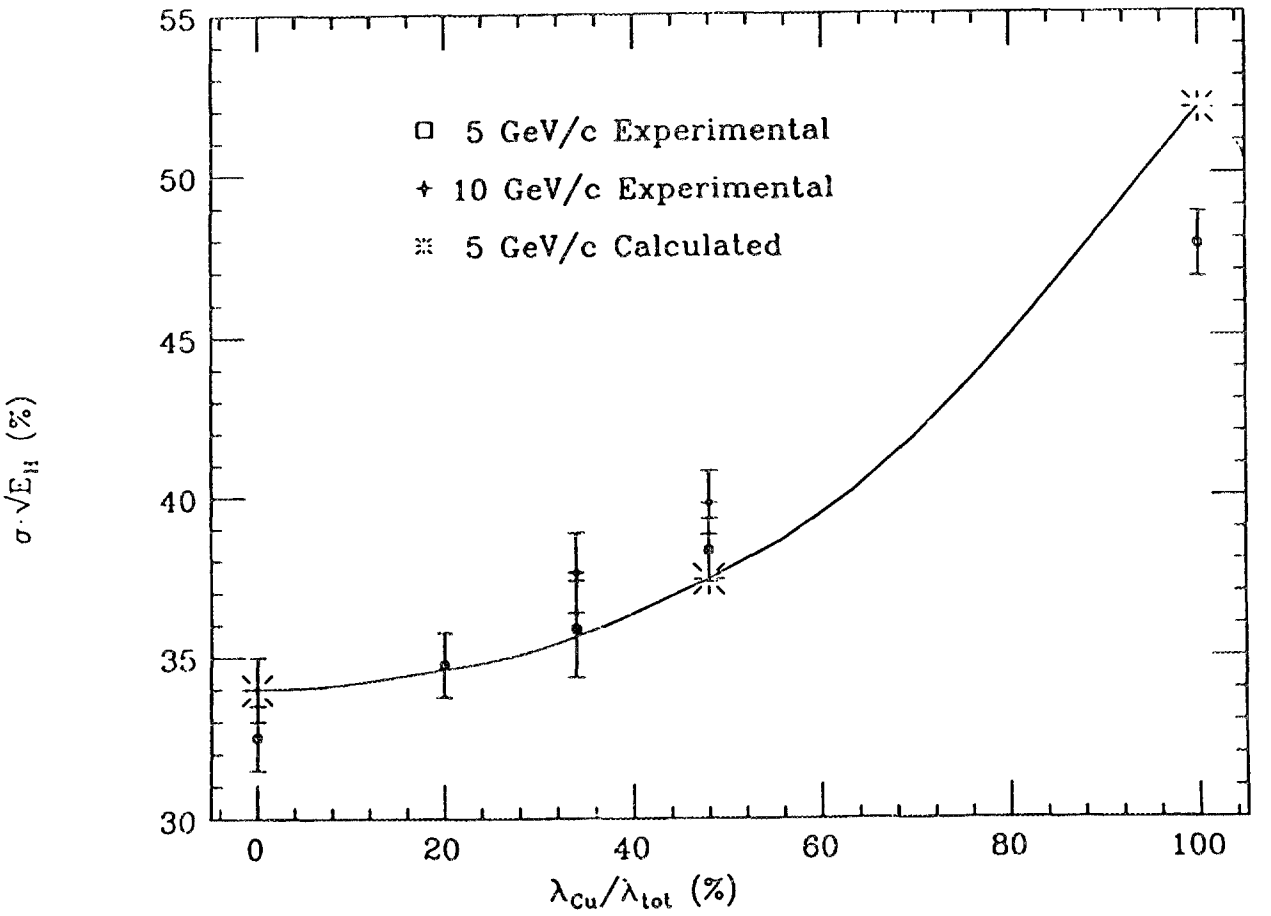

Fig. 10. The comparison of the simulation[7] of the dependence of hadron energy resolution with uranium purity with the experimental measurements of the AFS Collaboration.[28]

In this same study, the response of a uranium-liquid argon calorimeter was found to be less compensating. This is demonstrated in Fig. 11. As Fig. 11 shows, the selection of events can alter the conclusion on the degree of compensation by reducing the e/h ratio and narrowing the energy distribution. References 7 and 8 pointed out this selection bias and the importance of selection in the analysis was confirmed by the experimenters.[29]

2.5 HYDROGENOUS MEDIA

This very different response of uranium calorimeters employing different readout media was interpreted in Refs. 7 and 8 to yield the new understanding of compensating calorimetry. The underlying phenomena responsible for the significant difference were explained in terms of three basic differences of the sampling materials.[8] First, the neutron cross sections in hydrogen continue to rise below 1 MeV, while the cross sections in argon are falling (see Fig. 12). This in itself means that a larger fraction of the soft neutron energy will be deposited in the plastic scintillator than in the liquid argon. Secondly, the kinematic constraint

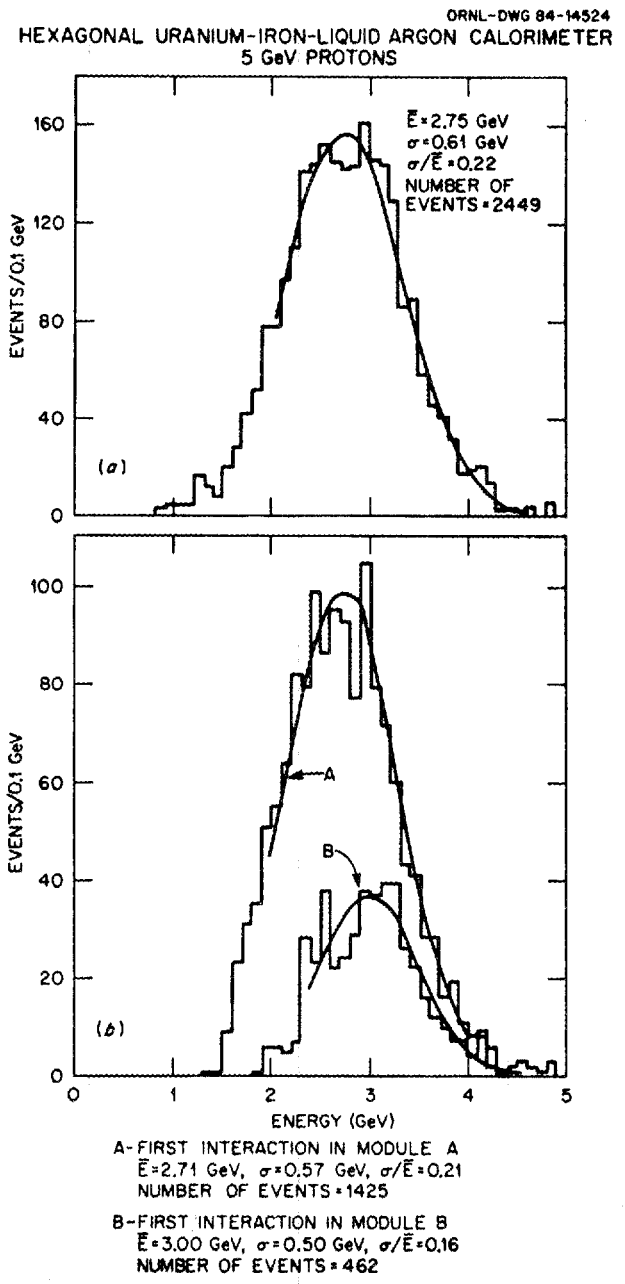

Fig. 11. The simulation[7] of the measured hadron energy distribution for the hexagonal uranium-liquid argon calorimeter of Ref. 21.

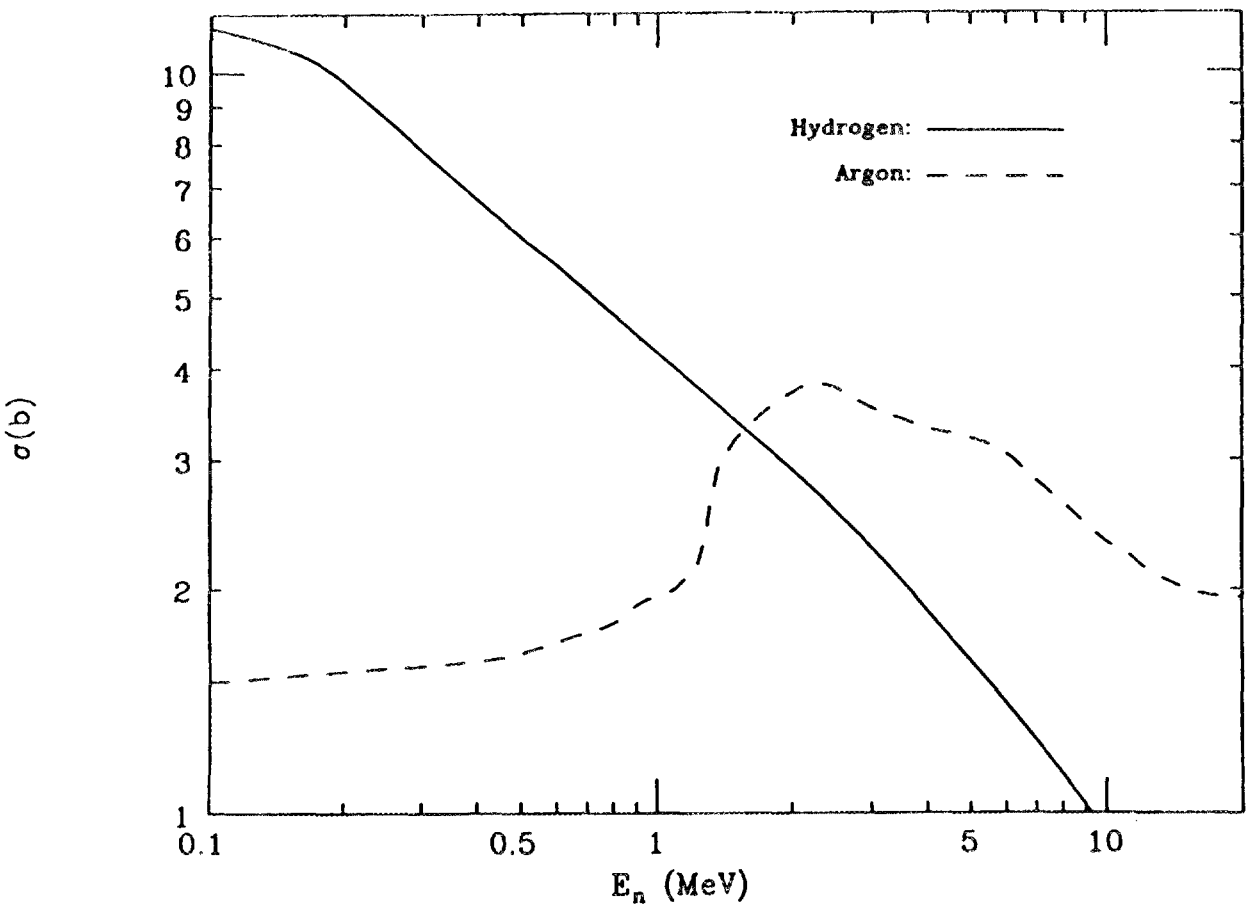

Fig. 12. Comparison of the neutron total cross sections in hydrogen and argon. The argon cross section represents the average value in the regions of much structure. (These are approximate curves presented only for comparison.)

on the energy transferred in a neutron-nucleus collison highly favors the transfer of energy to a lighter nucleus. The maximum possible recoil energy ($E_R \mid_{max}$) transferred from an incoming nonrelativistic neutron of kinetic energy E_n to a recoil nucleus of atomic weight A can be shown[30] simply from conservation of momentum and energy to be

$$E_R \mid_{max} = \frac{4A}{(1+A)^2} E_n. \tag{1}$$

This means that in neutron-hydrogen collisions, the full energy of the neutron can be transferred, while in neutron-argon collisions the maximum energy which can be transferred is ten percent of the neutron energy. Thirdly, the energy coupling is even more suppressed in liquid argon due to the saturation which occurs in regions of dense energy loss. In scintillators this phenomenon has been studied for many years and was modelled by Birks[31] in a form that has come to be known as Birks' Law:

$$\frac{dL}{dx} = \frac{S\frac{dE}{dx}}{1 + kB\frac{dE}{dx}}, \tag{2}$$

where $\frac{dL}{dx}$ is the light yield per unit path length, $\frac{dE}{dx}$ is the specific energy loss for the charged particle, S is the normal scintillation efficiency, and the kB parameter describes the quenching which occurs for high density ionization. Typical kB factors for scintillators are 0.01-0.02 gm/cm^{-2} MeV^{-1}. Following the suggestion of Ref. 7, it has become customary to express the columnar recombination[32] which results in saturation in liquid argon ionization sampling calorimeters also in the form of the Birks' Law. In this form the equivalent kB factor for liquid argon is about 0.005 gm/cm^{-2} MeV^{-1}, that is less saturating than scintillator. While the intrinsic saturation in liquid argon is less than in scintillator, the kinematic constraint on the energy transfers in neutron-nucleus collisions leads to a greater suppression of the transfer of neutron energy to observable signal. In liquid argon the highly ionizing recoil nuclei receive only one-tenth the relative energy of the less highly ionizing recoil protons in scintillator.

Qualitatively it is easy to see why the saturation has so much more of an effect by examining the calculations of Refs. 7 and 8. The 5 GeV protons studied in those calculations were found to deposit 402 MeV into the liquid argon gaps of 2.0 millimeters (the uranium thicknesses were 1.7 millimeters). However, due to saturation, only 308 MeV was detectable. The effect of this was to raise the e/h ratio to 1.2 from a potential value of 0.9 in the absence of saturation.[33] Of the 94 MeV lost to saturation, 72 MeV comes from collisions of the low energy ($<$ 20 MeV) neutrons. Therefore, the saturation of the energy delivered to the liquid argon has reduced the degree of compensation from an over-compensation condition to a value of 1.2. Note that this calorimeter was restricted in transverse dimension, particularly the uranium portion, and therefore a larger device would be expected to obtain smaller values of e/h. Furthermore, these calculations of e/h were subsequently confirmed by the experimenters.[29]

2.6 ELECTROMAGNETIC SAMPLING

It is important to recognize the significant effects of reduced electromagnetic response in calorimeters composed of high Z radiator structures.[11] These "electromagnetic sampling inefficiencies" have been explained as resulting from the preferential absorption of low energy photons ($<$ 1 MeV) in the high Z material and the effective electron path length stretching in the inactive media resulting from enhanced multiple scattering in the high Z material.[6,9,13] Figure 13 displays how the preferential absorption of the low energy photons in the high Z material comes about. Here the photon mass attenuation coefficient multiplied by the fraction of primary photon energy loss for argon and for lead can be seen.[34] Clearly in the high Z material, the relative absorption at low energy, say $\sim$ 100 keV, is much more effective in stopping the photons. The role of multiple scattering has also been clearly demonstrated by examining the effect of turning off multiple scattering in the electron-gamma shower program EGS.[35] Such calculations for 1 GeV electron showers in uranium liquid argon sampling calorimeters show an increase of 10% in the signal deposited in the liquid argon as the electron path length stretching disappears.[6,9] The magnitude of this "electromagnetic sampling inefficiency" is often measured by comparing the response of a calorimeter for incident electrons to that anticipated for minimum ionizing particles. The fictitious fully contained minimum ionizing particles can be measured by scaling up the response of the calorimeter to muons. Such measurements find the ratio of average electron pulse height to

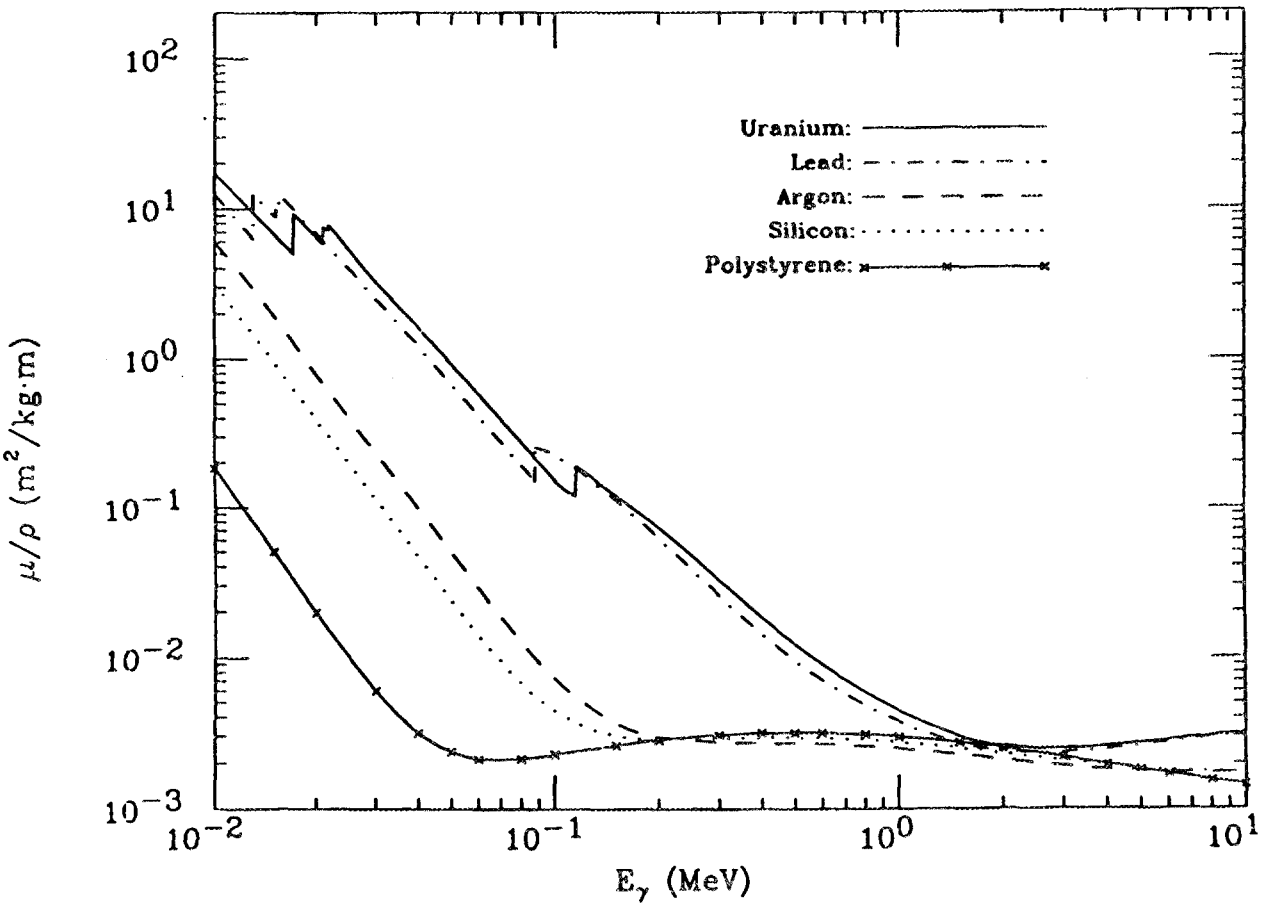

Fig. 13. Comparison of the photon mass attenuation coefficients multiplied by the fraction of primary photon energy loss for polystyrene, silicon, argon, lead, and uranium.

the pulse height for the minimum ionizing particle to be roughly 0.6 to 0.7 for calorimeters constructed with high Z radiators. The magnitude of this effect led us to the prediction "that a lead calorimeter may also give EM/HAD $\approx$ 1."[12] This prediction has now become reality. Figure 14 shows the resolution as a function of energy for a lead-scintillator compensating calorimeter built with scintillator thicknesses of one-quarter the lead thicknesses, a ratio designed to give the optimal electon to hadron ratio.[15] The reported e/h ratio for this device is 1.05 $\pm$ 0.04 for energies over 10 GeV. Caution should be exercised, however, since this analysis is based on events selected by energy deposition. This selection could emphasize the electromagnetic parts of the hadronic shower and yield a biased e/h ratio.

The understanding of the underlying phenomenology of compensating calorimeters is on solid ground and calculations can be done reliably. The requirements of the future hadron colliders demand that wise use be made of this understanding.

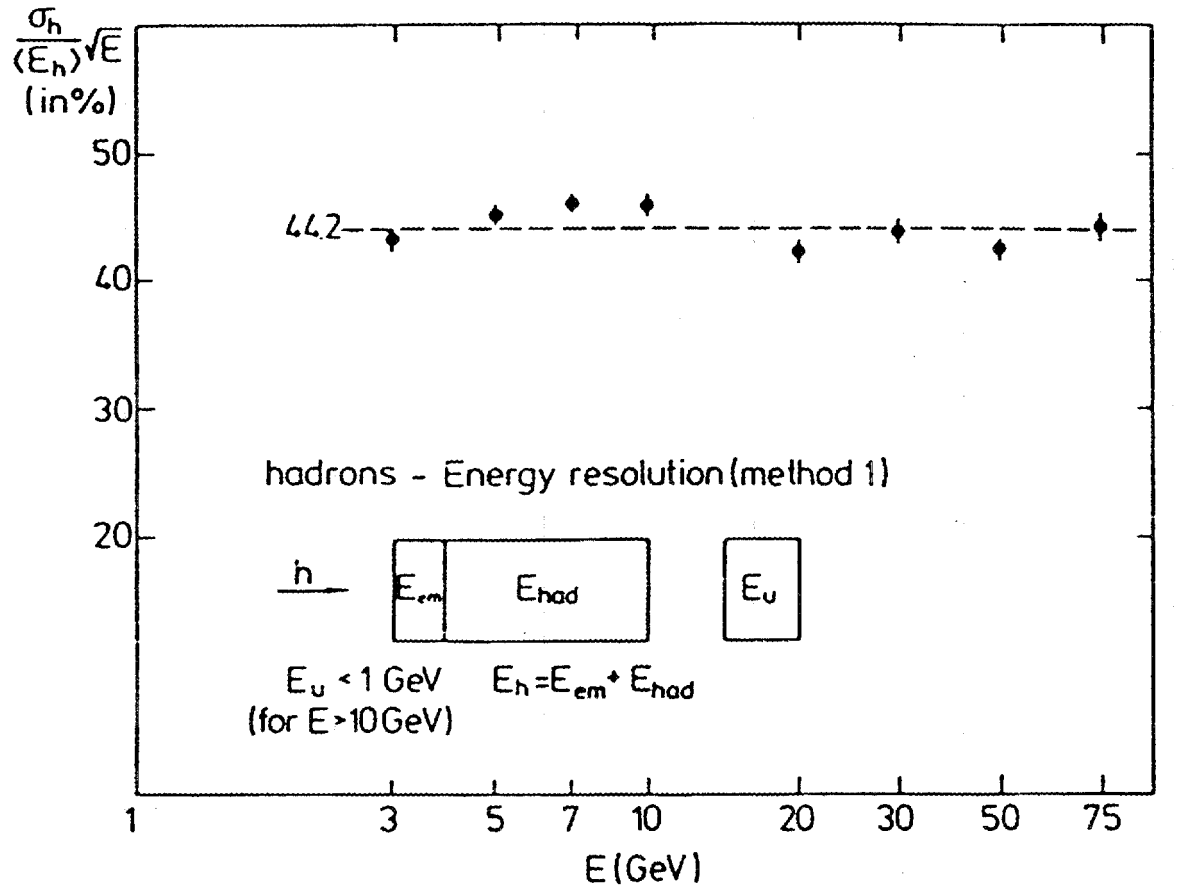

Fig. 14. Energy dependence of the hadron energy resolution of the compensating lead calorimeter presented in Ref. 15.

3. THE OPTIONS FOR CALORIMETRY AT FUTURE COLLIDERS

Many alternative calorimeter configurations are being considered for systems at the future colliders. Table 3 summarizes many of the options being considered for the SSC.[36] One general feature of this list is the inclusion of a high Z radiator, either lead or uranium, in each approach. This acknowledges the role of the electromagnetic sampling inefficiency in the compensation mechanism. Two of the four readout choices are highly hydrogenous, the TMP or TMS system and the scintillator approach. This explains the expectation for an e/h of 1.0 for each of these. While liquid argon as a readout doesn't get high marks on the list for hermeticity, speed, or e/h, its success as a proven, operating system in present experiments must be respected.[37,38]

Table 3
Table of calorimeter candidates for the Supercollider as presented in Ref. 34.*

Calorimeter Candidates[34]						
Absorber	Sampler	e/h	$\Delta E/E(had)$	Hermeticity	Speed	Major Problems
Uranium	Liq. argon	$\approx$1.1	$45\%/\sqrt{E}$	*	*	Hermeticity, e/h
Lead	Liq. argon	$\approx$1.3	$55\%/\sqrt{E}$	*	*	e/h
Uranium	TMS/TMP†	$\approx$1?	$30\%/\sqrt{E}$?	**?	*	Many??,S/N
Lead	TMS/TMP	$\approx$1?	$30\%/\sqrt{E}$?	**?	*	See above
Uranium	Scintillator	1	$35\%/\sqrt{E}$	*	***	Granularity,rad. dam.
Lead	Scintillator	1	$40\%/\sqrt{E}$?	*_***††	***	Same as above
Uranium	Silicon	1?	$45\%/\sqrt{E}$	***	**?	Cost,rad. damage

*The listing here for uranium-silicon omits the reference to CH_2 which originally was proposed, as the calculations presented in this paper indicate that CH_2 will be ineffective in producing compensation via proton knockin. Nevertheless, the CH_2 is probably unnecessary as the calculations of this work find large coupling of neutron energy to the silicon.

†Many of the properties of TMS/TMP are not sufficiently known for accurate predications.

†† If used with (so far unproven) scintillating fiber readout rather than the usual plates and wavelength shifters.

Many of the various approaches for SSC/LHC calorimeters have been considered in other papers presented at this conference. There is definitely a place at the future colliders for more than one technique as one examines the relative merits and demerits of each. To that end a calculational examination of the use of silicon in a calorimeter will be reported. These calculations are being persued in parallel with the experimental program.[39]

The option of employing silicon detector diodes as the sampling medium in hadron calorimeters has been suggested in a number of previous works.[40,41] Successful devices have been constructed and tested using silicon diodes in electromagnetic calorimeters.[42] The advantages of extending this success to hadron calorimetry are numerous.[43] As an ionization sampling calorimeter, a silicon readout calorimeter would be a system of absolute gain. Silicon is a nearly non-saturating medium so that sources can be used to get an absolute calibration of an energy scale. These devices can be operated at room temperature, eliminating the need for bulky and space wasteful cryostats required for other options. The signals have been shown to be relatively insensitive to magnetic fields. In principle the calorimeters can be made very compact due to the very thin sampling gaps required; since silicon diodes produce an electron-hole pair for every 3.7 eV deposited at room temperature, they require a much smaller sampling gap than most other systems. The technology of silicon diode fabrication makes fine lateral and longitudinal segmentation of silicon calorimeters easy and feasible. Finally, the property that provides the most promising feature of silicon diode readout is the speed of response. The intrinsic speed of normal diodes of thicknesses of 300 μm or so, is about 20 nanoseconds. Therefore, the speed of the front-end electronics is likely to limit the speed of response. However, achieving the optimal physics results at the future high rate colliders may well require calorimeters which exploit this intrinsic speed as fully as possible. It is for many of these reasons that the SICAPO Collaboration is working on the development of silicon hadron calorimeters.[39]

4. CALCULATIONS OF THE RESPONSE OF HADRONIC CALORIMETERS EMPLOYING SILICON DETECTOR READOUT

The understanding that now exists concerning compensating calorimeters can be applied to the silicon detector calorimeters. The fundamental question that needs to be addressed is what the e/h ratio for these silicon based calorimeters will be. One property of silicon that plays an important role in this study is the extreme linearity of silicon up to very large stopping power. That is, silicon exhibits very little saturation. It has been demonstrated that saturation prevents full compensation in currently designed uranium-liquid argon calorimeters, so this could be a very important factor in silicon calorimeters. Naively it is expected that very good results can be obtained for silicon calorimeters.

The linearity of response of silicon to large energy deposition densities is summarized in Figs. 15 and 16. Figure 15 shows the pulse height observed in a silicon detector for heavily ionizing heavy ions as a function of energy.[44] Here an extremely linear response for very high densities of ionization is presented. Figure 16 shows the relative response of a recoil ion of maximal energy in neutron scattering.[45] One sees that even for silicon ions as low as 100 keV nearly one-half of the deposited energy is detected as observable output signal. Given these evidences of very limited saturation in silicon detectors a very good response to some components of the low energy development of hadronic showers can be expected.

It is pedagogically useful to consider the differences between the response of silicon and liquid argon, since except for the saturation in liquid argon, full compensation could possibly be achieved. The three critical factors which were reviewed earlier to compare the neutron coupling to scintillator and liquid argon are useful to compare again here. First the neutron cross sections[46] are compared in Fig. 17. It can be seen that the cross section in argon falls for energies below a few MeV, while the cross section in silicon remains large and even rises below 500 keV. This will result in a larger energy deposition by low energy neutrons in silicon than is observed in liquid argon. The typical neutron energy spectrum which has been calculated in these studies[27] is also shown in this figure and illustrates the importance of the cross sections at the lowest energies. Secondly, the effect of the kinematic limitation on neutron energy transfer can be considered. Equation 1 shows that while only one-tenth of the neutron energy can be transferred in liquid argon collisions, the restriction on energy transfer is somewhat less restricted in silicon, being limited to about 13 percent. This should lead to an additional increase in the energy transferred to the silicon. Thirdly and finally, the very limited saturation which occurs in silicon will enable these increased neutron depositions to be more observable.

The potential for compensation with silicon certainly seems better than for liquid argon. To make quantitative predictions it is necessary to make use of a Monte Carlo code[22] system which takes into account all of the basic processes and examines the details of the shower development. As in our earlier studies, the Oak Ridge system CALOR has been applied to this problem. The details of this system are described in the Appendix. It has been assumed that the effective kB parameter

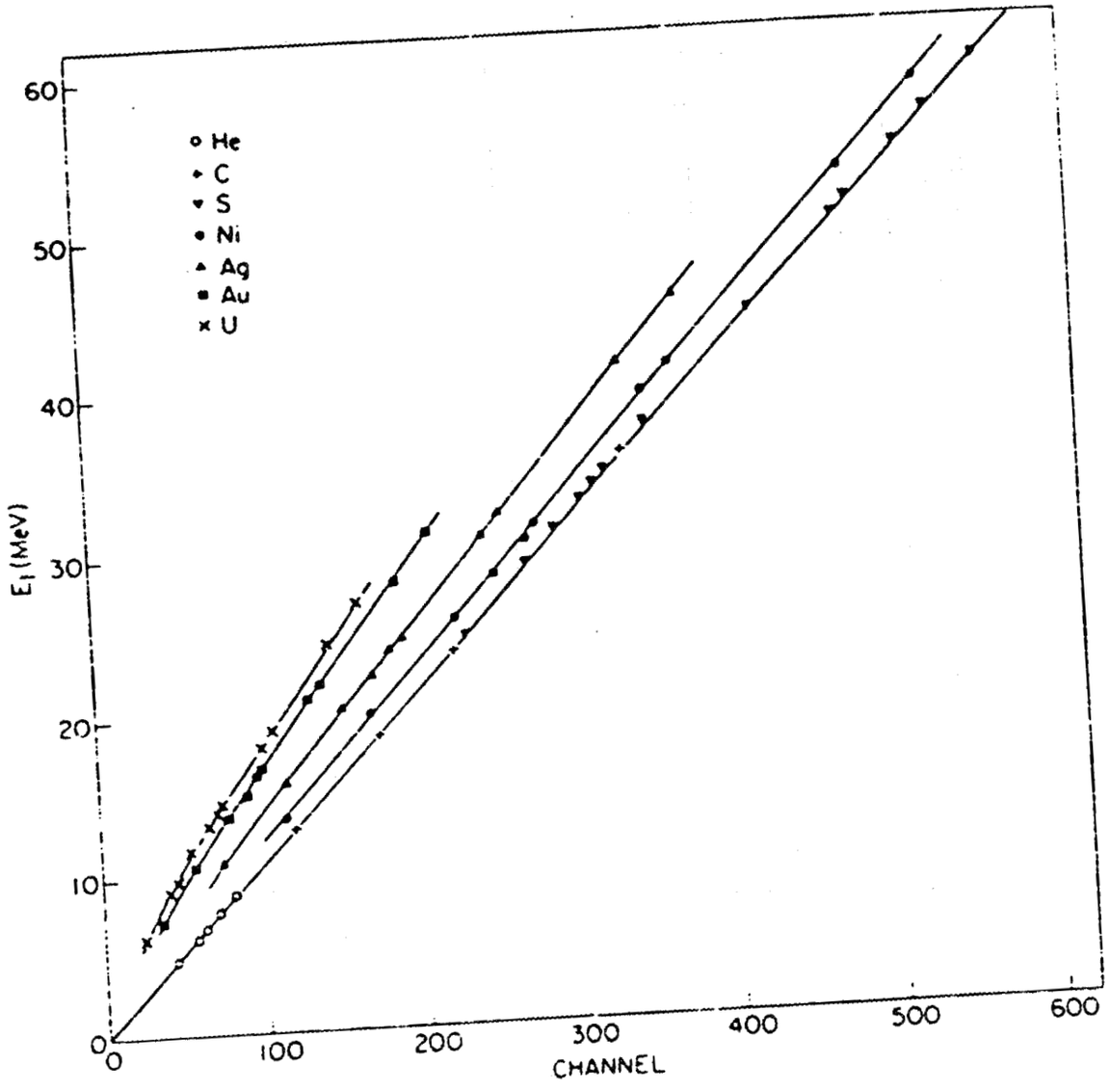

Fig. 15. The true energy of various ions versus the pulse height channel number from a silicon surface barrier detector. Data taken from Ref. 44.

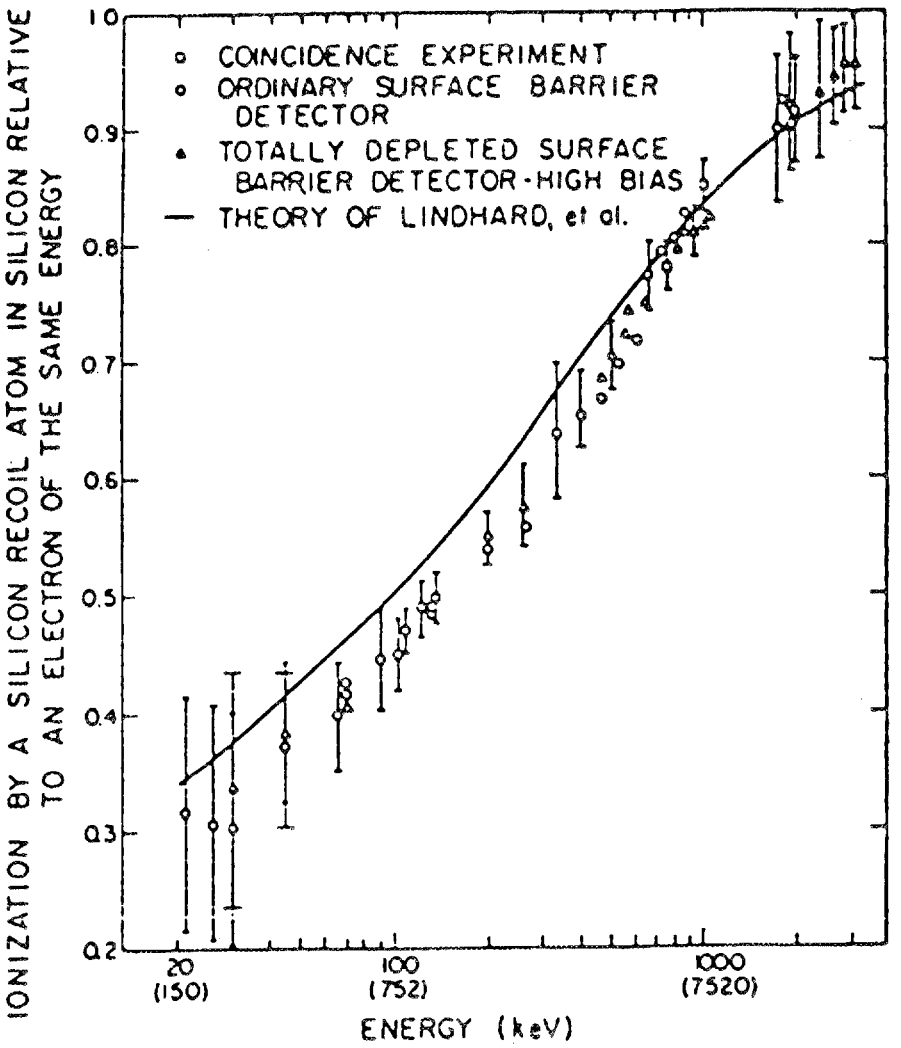

Fig. 16. Pulse height produced by a Si recoil atom relative to that of an electron of the same energy in Si as a function of Si recoil energy. The incident monoenergetic neutron energy necessary to produce the denoted recoil energy in a backscattering event is shown in parentheses. The solid line denotes predictions of Lindhard et al., as described in Ref. 45, the source of these data.

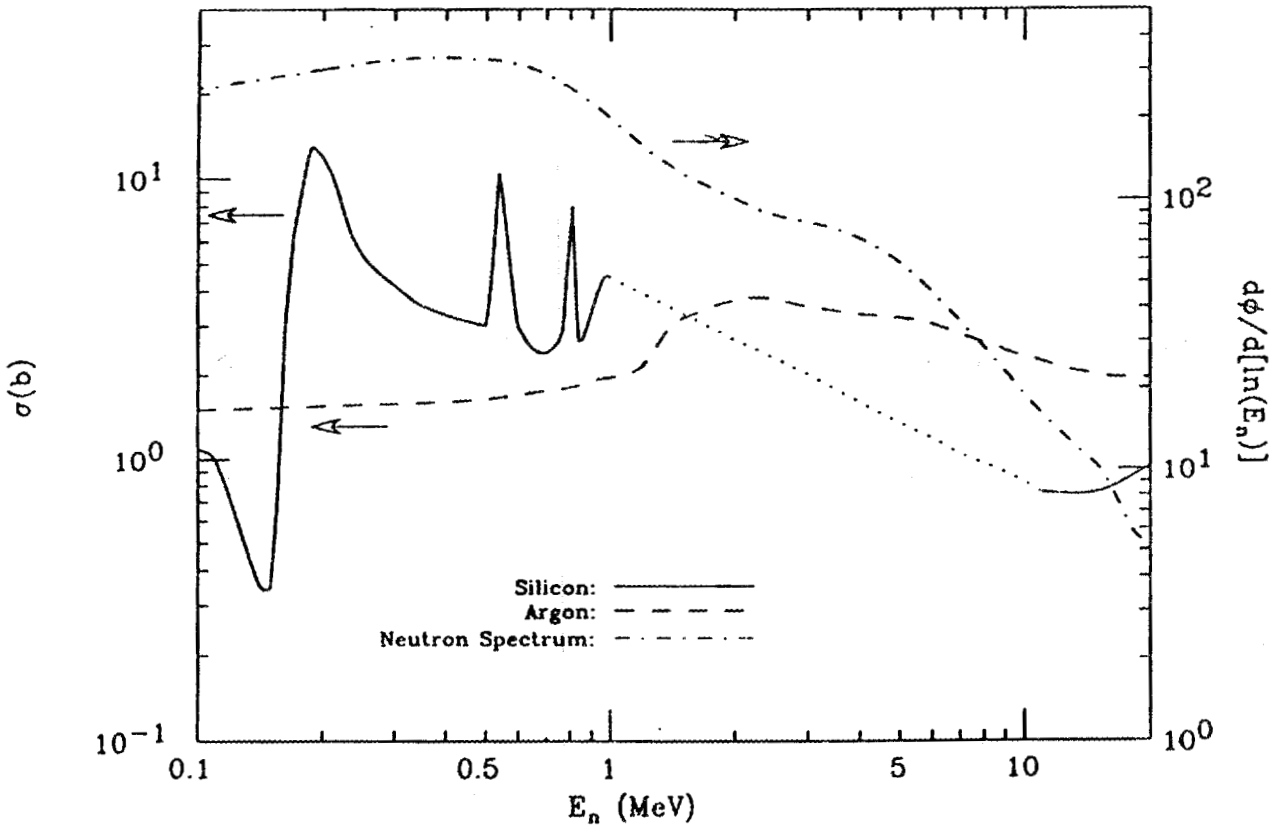

Fig. 17. Comparison of the neutron total cross sections in silicon and argon. The silicon and argon cross sections represents the averages in regions of much structure. (These are approximate curves presented only for comparison.) Also shown on this figure is the typical calculated neutron energy spectrum from Ref. 27.

in Birks' law is equal to 0, an approximation which should be very good for these studies. The e/h ratio will be only slightly underestimated in these calculations.

Figure 18 shows the calculated response distribution for 10 GeV π^- s incident on a silicon calorimeter with 5 millimeter thick uranium radiators and 400 μm fully depleted silicon detectors sandwich between two layers of 5 millimeter thick G10. Therefore, the total layer thickness is 15.4 millimeters and the depth of the stack extends for 150 readout and radiator layers. The transverse dimensions of the stack have been taken to be 100 × 100 cm^2. The charge collection is cut off after 50 nanoseconds. The resulting energy resolution (σ/E) is 21.5% and the e/h ratio is 1.07, close to compensation.[47] In fact the two layers of G10 in this stack are increasing the value of e/h as the neutron energy from the uranium is being deposited in the G10 through the large energy transfers via hydrogen. Additionally, significant transfers occur to the carbon and oxygen in the G10.

Figure 19 presents the event by event correlation of the energy detected in the silicon from the low energy (<20 MeV) neutrons to the binding energy lost in the

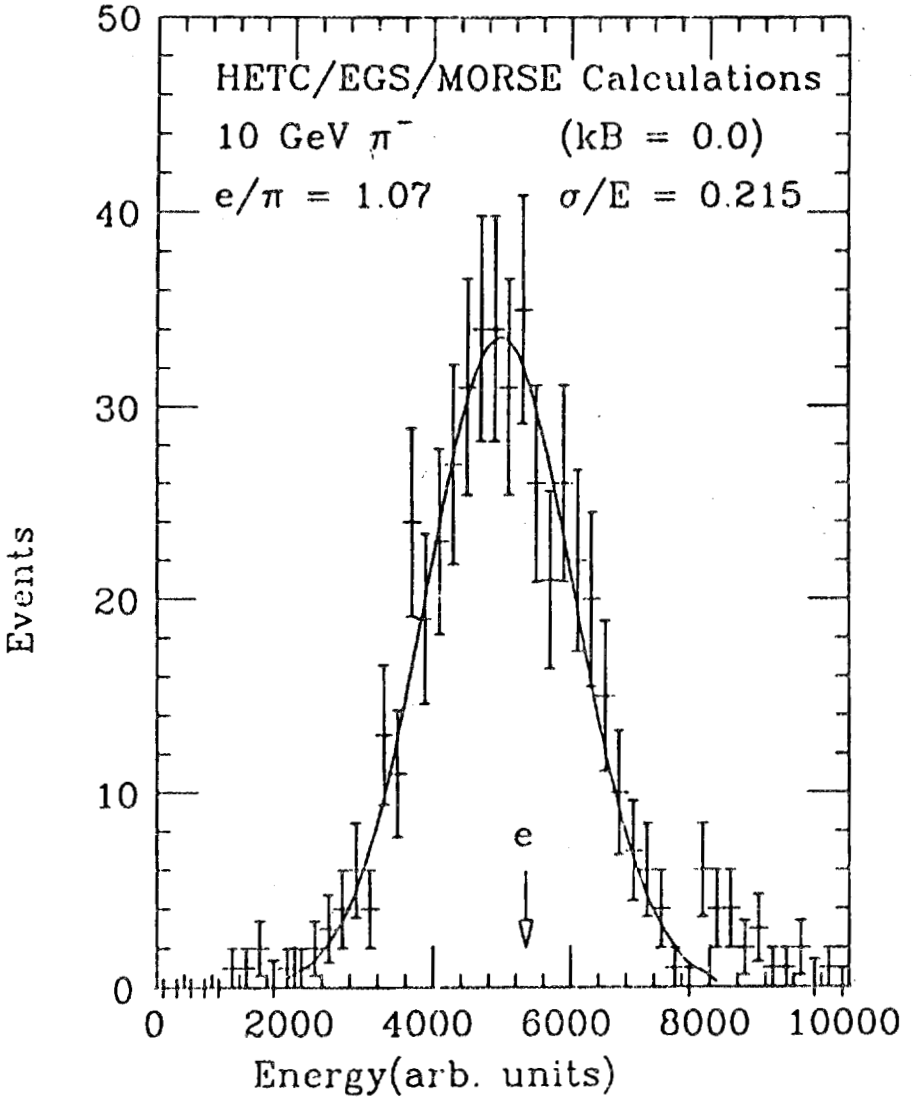

Fig 18. The calculation of the measured hadron energy distribution for 10 GeV π^- incident on a uranium-silicon calorimeter with 5 mm thick uranium radiators and 400 μm fully depleted detectors imbedded in 5 mm thick G10 supports.

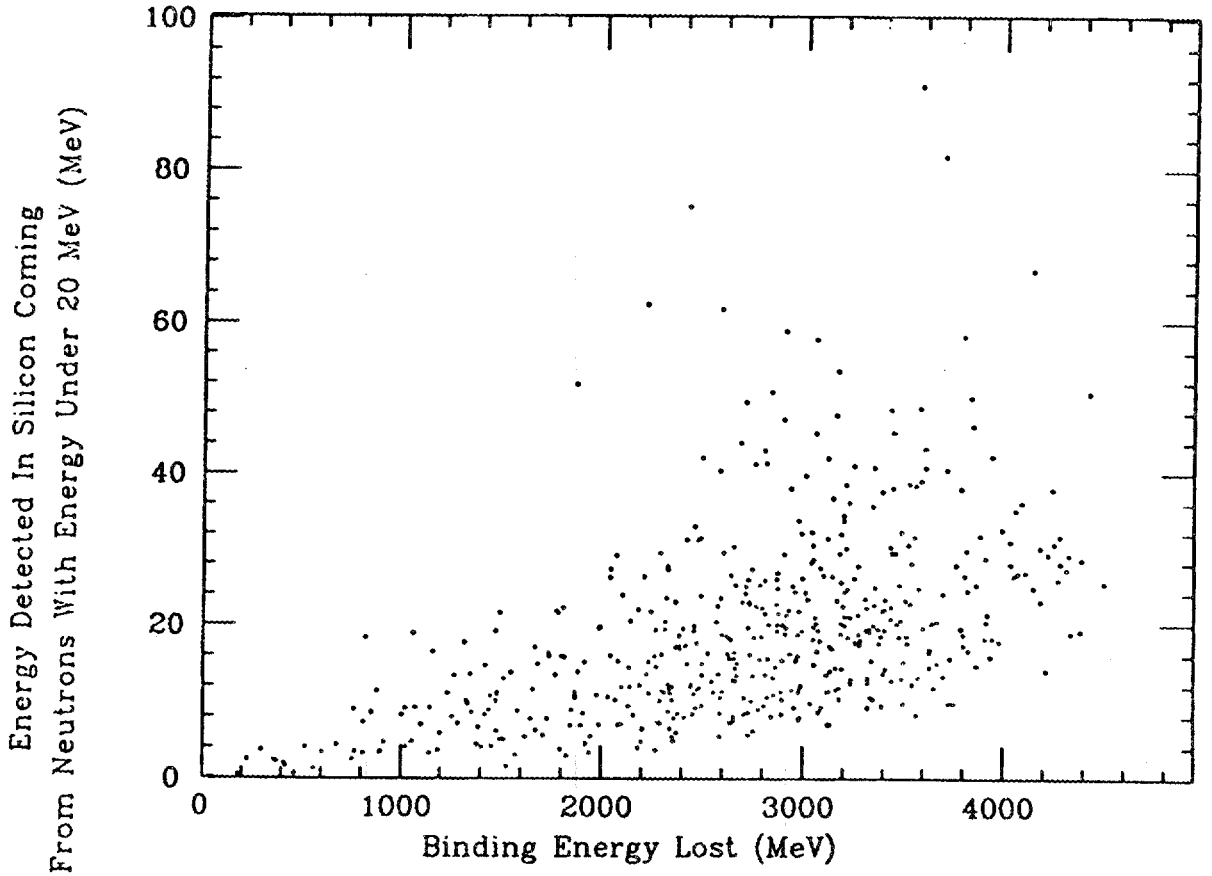

Fig. 19. The correlation of detected low energy (E < 20 MeV) neutron energy in the uranium-silicon calorimeter with the binding energy lost in the associated hadronic cascade. The small sampling fraction of the silicon is evident by the fluctuation of signal relative to the fluctuations in Fig. 6.

hadronic cascade. While the correlation is strong, this figure shows much larger fluctuations in detected energy than was seen in Fig. 6 for the uranium-scintillator calorimeter. This fluctuation depends on the number of neutrons actually detected. Given the very thin detection layers, the number of neutrons actually detected is small. Unlike the normal shower fluctuations which vary as $\sqrt{t_{cell}}$ and are dominated by the thickness of the radiator, the fluctuation on neutron response is dominated by the thickness of the silicon (t_{Si}), and scales as $\sqrt{t_{Si}}$. Therefore, the sampling fluctuations for the charged hadrons in the hadron cascades will be similar to any other readout medium, but the additional larger fluctuations on the neutrons will add to the width of the energy distribution, preventing excellent low energy resolution even for perfectly compensating calorimeters.

Figure 20 presents a series of calculated results for calorimeters constructed with 2 millimeter uranium radiators, followed by a layer of G10 of varying thickness and a 400 μm fully depleted silicon detector. As before, kB = 0, the time cut is

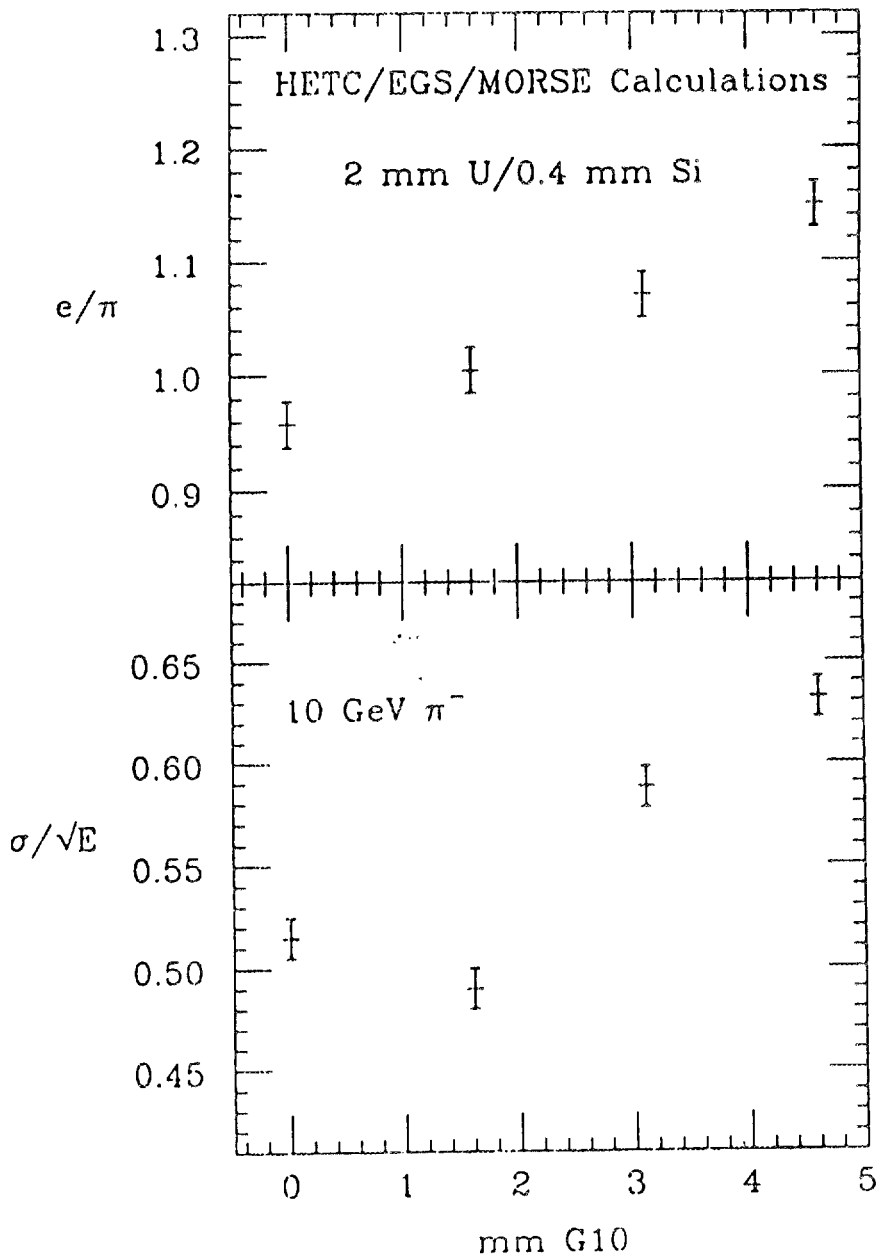

Fig. 20. The calculated variation of e/π and $\sigma/\sqrt{E}$ with the thickness of a G10 sheet placed between the 2 mm uranium plates in a uranium-silicon calorimeter and the silicon detectors. Without G10 a slight overcompensation condition exists, while as the thickness of G10 increases, the e/π ratio passes through 1. These calculations were done for incident 10 GeV π^-.

50 nanoseconds, and the transverse size is taken to be 100×100 cm^2. The stacks contain 330 layers of uranium, G10, and silicon. It can be seen that with no G10 the condition of overcompensation is obtained due to the sensitivity of the silicon detectors to very low energy particles. As the G10 is added, the e/h ratio increases due to the removal of neutron energy by the G10, meaning less energy is available to be deposited in the silicon. Naively, one might expect that the neutrons interacting in the G10 would contribute to the response of the silicon by knocking protons into the detectors. It has been proposed[7] that coupling a hydrogenous material to liquid argon, for example, would be a possible method for restoring its potential for compensation. However, the efficiency and range of the protons produced in the G10 is not large enough to have much of an effect on the total response of a detector of 400 μm thickness.[48] It can also be seen in Fig. 20 that the energy resolution reaches a minimum at approximately the point where the e/h ratio passes through one, as would be expected for a compensating calorimeter. The value of this resolution is not as small as the values achieved in scintillator because of the larger sampling fluctuations involved here, as described previously. Fig. 21 shows the distribution of measured energies for the 10 GeV π^- s incident upon the optimal device shown in Fig. 20, that with 1.6 millimeters of G10. The distribution shows a well-behaved, nearly Gaussian shape.

Several cases of silicon calorimeters have also been studied with different radiator materials, specifically one employing lead and one employing iron. For a lead calorimeter with 3 millimeter thick radiators and 400 μm fully depleted silicon detector with no air gaps and the same transverse geometrical constraints and time cuts as before, the calculated results yielded an expected e/h ratio of 1.16 with an energy resolution of $\frac{\sigma}{\sqrt{E}} = 47\%$ for 10 GeV π^- s. For an iron calorimeter with 7.5 millimeter radiators, followed by a 1.3 millimeter air gap, a 1 millimeter G10 layer, 400 μm of fully depleted silicon, a 1 millimeter G10 layer, and another 1.3 millimeter air gap, the e/h ratio increases to 1.29. For the 10 GeV π^-s the resolution is $\frac{\sigma}{\sqrt{E}} = 62\%$. Even for the iron, the role of low energy detection efficiency can be seen in the e/h ratio, and for the lead, the e/h ratio of 1.16 is within reach of the values which have been touted as acceptable for future "compensating" calorimeters.[36]

In connection with these calculations, the attractiveness of a low-Z radiator material such are iron should be pointed out. Iron has several advantages compared to uranium, for example. In iron, less binding energy loss in inelastic collisions is realized, and this factor therefore contributes less to the energy spread than in calorimeters employing higher Z radiators. Secondly, connected with this is the fact that fewer neutrons are produced in these collisions and the produced neutrons are a source of radiation damage at high luminosity colliders. Thirdly, uranium is more expensive than iron.[49] Finally, uranium is difficult to obtain and to work with. In spite of these advantages for low Z over high Z, it is difficult to anticipate a practical design of a compensating iron calorimeter. As we have seen, the electromagnetic sampling inefficiencies are an important factor in achieving compensation. These effects are small in iron due to the small value of the charge of the iron nucleus. As a result, the response of an iron calorimeter to electromagnetic and non-electromagnetic energy deposition is much different, yielding a large fluctuations in the pulse height distribution. The small binding energy losses are overcome by the fluctuations between electromagnetic and non-electromagnetic energy. It is conceivable to imagine a combination of low-Z and high-Z material which will

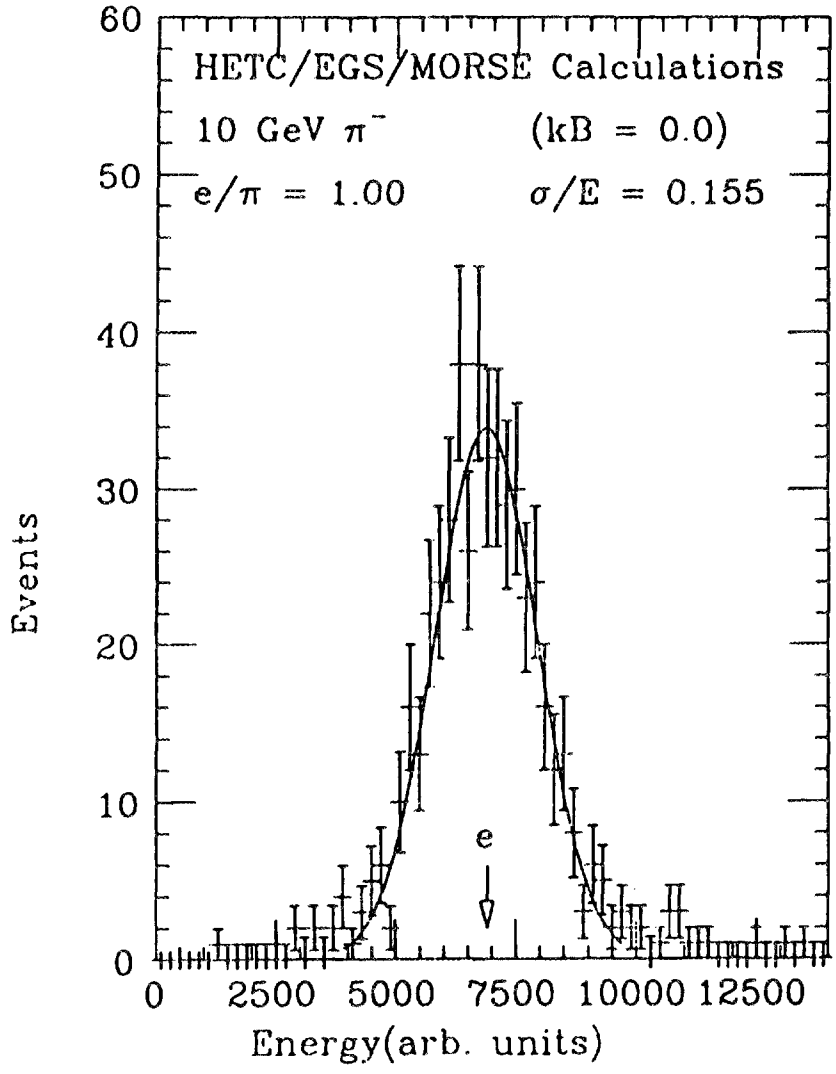

Fig. 21. The calculated measured hadron energy distribution for 10 GeV π^- incident on a uranium-silicon calorimeter with 2 mm thick uranium radiators and 400 μm fully depleted detectors with a 1.6 mm G10 layer behind the uranium and in front of the silicon layers.

combine the advantages of each material and approach a resolution determined by the small binding energy losses of iron.

It is important to keep in mind some of the other unsolved problems of silicon readout hadron calorimeters. One very important concern is the tolerance, or potential lack thereof, of silicon to the radiation environment that the future high luminosity, high rate colliders will present. Recent work in this area has illuminated the situation and shown that it is not as dismal as was earlier feared. The improvement in tolerance to neutrons which is expected to occur with higher resistivity materials[50] has been demonstrated.[51] Strong self-annealing effects have been observed following the exposure of such devices to intense neutron sources.[52,53] Finally, a study of the expected effects of the radiation environment

of the SSC[20] on the operation of an imagined detector (the compact solenoidal detector) employing silicon calorimeters,[54] including the best understanding of these resistivity dependence effects and self annealing, has concluded that such an operation appears practical.[55] Further radiation effects tests are called for, but the situation looks manageable.

The second major area of concern is in the cost of providing the detectors for such a project. The total area of silicon required for the calorimeter of the compact solenoidal detector is 20 million cm^2. To make such a project realizable means that devices must be available for about two dollars per cm^2. Presently, devices are being ordered for 6-12 dollars per cm^2 so that an improvement of a factor of 3-6 is needed. The prospects for such an improvement for a detector of the scale of the compact solenoidal detector look good, however.[56]

One final issue of concern must be mentioned and that is the problem of how to read out the detectors while preserving the intrinsic speed. Radeka and Rescia have noted the design constraints on speed for ionization sampling calorimeters.[57] Achieving calorimeter responses of $\sim$20 nanoseconds requires that the product of detector capacitance and inductance of the connections be kept below 4 $nsec^2$. For a cell of one nanofarad this means the inductance of the connections must be kept below 4 nanoHenries, which requires less than a centimeter of lead for practical means. The compact solenoidal detector design, in fact, proposes about 1 nanofarad per layer of silicon detectors in the hadron calorimeter. Therefore, preserving the intrinsic speed will probably require the mounting of active elements on every layer. While this involves millions of transistors, it appears achievable. The combining of pads in series is also a possible means to achieve reduced capacitance and is being pursued by the SICAPO Collaboration. One must also keep in mind the significant noise cost which must be accepted to preserve the speed. This probably will prevent calibration of the calorimeter with muons, but shouldn't limit the energy resolution of real physics signatures.

5. CONCLUSIONS

The new understanding of compensating calorimeters which was introduced four years ago has now been experimentally confirmed in numerous tests. One important element of that understanding was the role of saturation in uranium-liquid argon calorimeters. High rate, high energy colliders are going to demand compensating, fast, finely segmented calorimeters. Our calculations indicate that the near absence of saturation in silicon should lead to compensation. Silicon's other attractive features (speed, ease of segmentation, and absolute gain calibration) make it an extremely attractive approach. The many other calorimeter approaches also have strengths which should be examined. The current status of our understanding of calorimetry puts us in a strong position to exploit the technique at the next generation of colliders.

6. APPENDIX: THE METHOD OF CALCULATION

The calculations reported here have been performed with the CALOR computer code system following approximately the procedures used in previous calculations.[58,26,7,8] A flow diagram of the codes in CALOR is given in Fig. 22. The three-dimensional, multimedia, high-energy nucleon-meson transport code (HETC)[59] was used, with modifications to obtain a detailed description of the nucleon-meson cascade produced in the devices considered in this paper. This Monte Carlo code takes into account the slowing down of charged particles via the continuous slowing down approximation, the decay of charged pions and muons, inelastic nucleon-nucleus and charged-pion-nucleus (excluding hydrogen) collisions through the use of the intermediate-energy intranuclear-cascade-evaporation (MECC) model ($E < 3$ GeV) and a scaling model ($E > 3$ GeV), and inelastic nucleon-hydrogen and charge-pion hydrogen collisons via the isobar model ($E < 3$ GeV) and phenomenological fits to experimental data ($E > 3$ Gev). Also accounted for are elastic neutron-nucleus ($E < 100$ Mev) and elastic nucleon and charged-pion collisions with hydrogen.

The intranuclear-cascade-evaporation model as implemented by Bertini is the heart of the HETC code.[60] This model has been used for a variety of calculations and has been shown to agree quite well with many experimental results. Even when agreement is not very good, the results produced by this model can lead the user to make correct decisions. The underlying assumption of this model is that particle-nuclear interactions can be treated as a series of two-body collisions with the nucleus and that the location of the collision and resulting particles from the collision are governed by experimental and/or theoretical particle-particle total and differential cross-section data. The types of particle collisions included in the calculations are elastic, inelastic and charge exchange. The model incorporates the diffuseness of the nuclear edge, the Fermi motion of the bound nucleons, and exclusion principle, and a local potential for nucleons and pions. The density of the neutrons and protons within the nucleus (which is used with the total cross section to determine interaction locations) are determined from the experimental data of Hofstadter.[60] Nuclear potentials are determined from these density profiles by using a zero-temperature Fermi distribution. The total well depth is then defined as the Fermi energy plus 7 MeV. Following the cascade part of the interaction, there is excitation energy left in the nucleus. This energy is treated by using an evaporation model which allows for the emission of protons, neutrons, deuterium, helium, and tritium. Fission induced by high-energy particles is accounted for during this phase of the calculation by allowing it to compete with evaporation. Whether or not a detailed fission model is included has very little effect on the total number of secondary neutrons produced in HETC.

The source distribution for the electromagnetic cascade calculation is provided by HETC. It consists of photons from neutral pion decay, electrons and positrons from muon decay (although this is usually not of interest in calorimeter calculations because of the long muon lifetime), deexcitation gamma rays from inelastic nuclear collisions and fission gamma rays. Since the discrete decay energies of the deexcitation gammas are not provided by HETC and only the total energy is known, individual gamma energies are obtained by uniformly sampling from the available

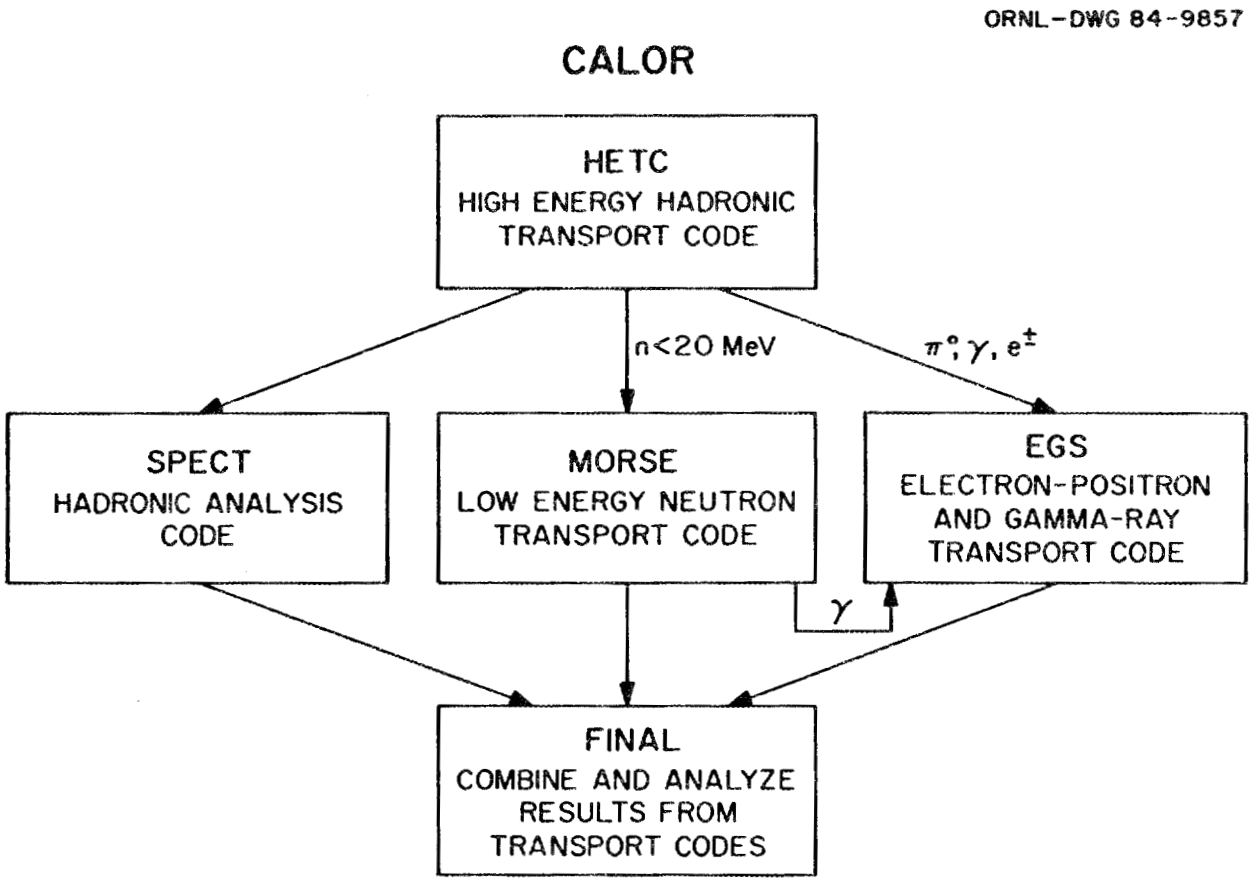

Fig. 22. Flow diagram of the CALOR computer code system.

energy until it is completely depleted. The transport of the electrons, positrons, and gammas from the above sources is carried out using the EGS system.[35]

Neutrons which are produced with energies below 20 MeV are transported using the MORSE[61,62] Monte Carlo transport code. The neutron cross sections used by MORSE were obtained from ENDF-B/IV. Gamma rays (including those from capture, fission, etc.) produced during this phase of the calculations are stored for transport by the EGS code. The MORSE code was developed for reactor application and can treat fissioning systems in detail. This ability is very important since a majority of the fission compensation results from neutrons with energies less than 20 MeV. Time dependence is included in MORSE, but since neither HETC nor EGS has a timing scheme incorporated, it has been assumed that no time passes for this phase of the particle cascade. Therefore, all neutrons below 20 MeV are produced at t = 0. General time cuts used in the MORSE code are 50 ns for scintillator and 100 ns for liquid argon.

The nonlinearity of the light pulse or charge collected (L) due to saturation effects is taken into account by the use of Birks' law:[31]

$$\frac{dL}{dx} = \frac{S\frac{dE}{dx}}{1 + kB\frac{dE}{dx}}, \tag{3}$$

where kB is the saturation constant. For the scintillators studied, kB = 0.01 or 0.02 g/cm^{-2}/MeV^{-1}, while for the liquid argon kB = 0.0045 g/cm^{-2}/MeV^{-1}. The liquid argon value is based on the data that a 5-MeV alpha particle gives the same signal as a 1.25-MeV electron.[21,32] This takes into account the loss of signal resulting from recombination effects in the ionization column. For electrons at all energies, it is assumed that kB = 0.

7. ACKNOWLEDGEMENTS

We would like to thank the organizers of the International Conference on Advanced Technology and Particle Physics for inviting us to Villa Olmo to present our work at the conference. We are greatly indebted to William M. Bugg for support and encouragement which has contributed significantly to the success of this work. Finally we would like to thank Scott Hendickson, Sharon L. White, and Coralee Zeigler for technical assistance during the preparation of this manuscript.

REFERENCES

1. S. Iwata, Nagoya University Report, DPNU-3-79 (1979).
2. U. Amaldi, Phys. Scripta 23, 409 (1981).
3. C.W. Fabjan and T. Ludlam, Ann. Rev. Nucl. Part. Sci. 32, 335 (1982).
4. C.W. Fabjan, Lectures given at the NATO Advanced Studies Institute on Techniques and Concepts in High Energy Physics, St. Croix, Virgin Islands, USA, CERN-EP/85-54 (1985).
5. J.E. Brau and T.A. Gabriel, SLD-New Detector Note no. 119, May 22, 1984.
6. J.E. Brau, "A Monte Carlo Investigation of Compensation in Uranium Calorimeters," Proceedings of the September 1984 Seattle meeting of the SLD Collaboration.
7. J. Brau and T.A. Gabriel, "Monte Carlo Studies of Uranium Calorimetry," Nucl. Instum. and Methods A238, 489 (1985).
8. T.A. Gabriel, B.L. Bishop, J. Brau, A. DiCiaccio, M. Goodman, and R. Wilson, "Compensation Effects in Hadron Calorimeters," IEEE Trans. Nucl. Sci. NS-32, 1 (1985).
9. J.E. Brau, "A Monte Carlo Investigation of Compensation in Uranium Calorimeters," Proc. Workshop on Compensated Calorimetry, Pasedena (1985) CALT-68-1305.
10. T.A. Gabriel, "Codes, Models, and Cross Sections for use in Analyzing Compensated Calorimeters," Proc. Workshop on Compensated Calorimetry, Pasedena (1985) CALT-68-1305.
11. P.M. Mockett, Proceedings of the Eleventh SLAC Summer Institute on Particle Physics, July 1983, ed. Patricia M. McDonough, SLAC-267 (1984).
12. H. Gordon and P. Grannis, "Calorimetry for the SSC," Proceedings of the 1984 Summer Study on the Design and Utilization of the SSC, Snowmass, Colorado, p. 591 (1984), eds. R. Donaldson and J.G. Morfin.
13. H. Brüeckmann, "Hadron Calorimetry - A Puzzle of Physics", Proc. Workshop on Compensated Calorimetry, Pasedena (1985) CALT-68-1305.
14. G. d'Agostini et al, "Experimental Study of Uranium Plastic Scintillator Calorimeters", NIKHEF-H/88-4 (April 1988).
15. E. Bernardi et al, Nucl. Instrum. and Methods A262, 229 (1987).
16. C. Leroy, Y. Sirois, and R. Wigmans, Nucl. Instrum. and Methods A252, 4 (1986).
17. R. Wigmans, "On the Energy Resolution of Uranium and Other Hadron Calorimeters," Nucl. Instrum. and Methods A259, 389 (1987).
18. H. Brüeckmann et al, Nucl. Instrum. and Methods A263,136 (1988).

19. D. Soper, presentation at the Workshop on Experiments, Detectors, and Experimental Areas for the Supercollider, Berkeley, California, 1987.

20. D. Groom (ed.), "Radiation Levels in the SSC Interaction Regions," SSC-SR-1033 (1988).

21. C.W. Fabjan et al, Nucl. Instrum. and Methods 141, 61 (1977);

22. T.A. Gabriel, "The High Energy Transport Code HETC," ORNL/TM-9727 (1985).

23. G. Rudstam, Z. Naturforsch. 21a,1027 (1966); G. Rudstam, Nucl. Phys. A126, 401 (1969).

24. This count does not include neutron nuclear collisions for neutrons below 20 MeV.

25. Note that the prompt gammas mentioned above, although ineffective, are included in the calculations described here.

26. T.A. Gabriel, Nucl. Instrum. and Methods 150, 145 (1978).

27. J.E. Brau and T.A. Gabriel, "Calculations of Neutron Flux in Iron and Uranium Calorimeters," Appendix 15 of "Radiation Levels in the SSC Interaction Regions," SSC-SR-1033, edited by D. Groom (1988).

28. O. Botner et al, IEEE Trans. Nucl. Sci. NS-28, 510 (1981); O. Botner et al, Nucl Instrum. and Methods 179, 145 (1981).

29. P. Rehak, Proc. Workshop on Compensated Calorimetry, Pasedena (1985) CALT-68-1305.

30. G. Knoll, Radiation Detection and Measurement, John Wiley and Sons, New York (1979), p. 570.

31. J.Birks, Proc. Phys. Soc. A64, 874 (1951).

32. W. Hofmann et al, Nucl. Instrum. and Methods 135, 151 (1976).

33. This value calculated for this calorimeter represents the lowest obtainable value for e/h. Note that liquid argon could be made to compensate if a method were available to retrieve all of the deposited energy.

34. J.H. Hubbell, Int. J. Appl. Radiat. Isot. 33, 1269 (1982); J.H. Hubbell, H.A. Gimm, and I. Overbo, J. Phys. Chem. Ref. Data 9, 1023 (1980); E. Storm and H.I. Israel, Nucl. Data Tables A7, 565 (1970).

35. R.L. Ford and W.R. Nelson, "The EGS Code System Computer Programs for the Monte Carlo Simulation of Electromagnetic Cascade Showers (Version 3)," SLAC-0210 (1978).

36. M.G.D. Gilchriese, Proceedings of the 1987 SLAC Summer Institute on Particle Physics.

37. S. Wimpenny, International Conference on Advanced Technology and Particle Physics, Villa Olmo, Lake Como, Italy, June, 1988.

38. C. Bromberg, International Conference on Advanced Technology and Particle Physics, Villa Olmo, Lake Como, Italy, June, 1988.

39. SICAPO Collaboration, presented by C. Leroy and F. Lemeilleur, International Conference on Advanced Technology and Particle Physics, Villa Olmo, Lake Como, Italy, June, 1988.

40. T. Kondo, Y. Watanabe, and S. Kim, Proceedings of the 1984 Summer Study on the Design and Utilization of the SSC, Snowmass, Colorado, p. 612 (1984), eds. R. Donaldson and J.G. Morfin.

41. P.G. Rancoita and A. Seidman, Nucl. Instrum. and Methods A263, 84(1988); S. Pensotti, P.G. Rancoita, A.Seidman, and L. Vismara, Nucl. Instrum. and Methods A265, 266(1988).

42. G. Barbiellini et al, Nucl. Instrum. and Methods A235, 55(1985); G. Barbiellini et al, Nucl. Instrum. and Methods A236, 316 (1985). M. Bormann et al, Nucl. Instrum. and Methods A240, 63 (1985); and A. Nakamoto et al, Nucl. Instrum. and Methods A251, 275 (1985).

43. T. Akesson et al, CERN-EP/87-88.

44. B.D. Wilkins, M.J. Fluss, S.B. Kaufman, C.E. Gross, and E.P. Steinberg, Nucl. Instrum. and Methods 92, 381 (1971).

45. A.R. Sattler, Phys. Rev. 138, A1815 (1965).

46. D. I. Garber and R.R. Kinsey, "Neutron Cross Sections; Volume II, Curves," BNL 325 (1976).

47. It is emphasized that the e/h ratio was calculated assuming no saturation in the silicon.

48. T.A. Gabriel, J.O. Johnson, and J.E. Brau, "MICAP: A Program for Low Energy Neutron, Ion, and Gamma-ray Transport and One of its Applications in Calorimeter Design: Hydrogen Knock-in as a Method for Achieving Compensation." Proceedings of the Workshop on Detector Simulation for the SSC, Argonne National Laboratory, August, 1987.

49. C. Baltay, J. Huston, and B.G. Pope, "Calorimetry for SSC Detectors," Proceedings of the 1986 Summer Study on the Physics of the Superconducting Supercollider, Snowmass, Colorado, p. 355 (1986), eds. R. Donaldson and J. Marx.

50. G.C. Messenger and M.S. Ash, The Effects of Radiation on Electronic Systems, Van Nostrand Reinhold, New York, (1986), p. 157.

51. H.W. Kraner, Z. Li, M. Momayezi, and K. Posnecker, International Conference on Advanced Technology and Particle Physics, Villa Olmo, Lake Como, Italy, June, 1988.

52. SICAPO Collaboration, presented by L. Vismara, International Conference on Advanced Technology and Particle Physics, Villa Olmo, Lake Como, Italy, June, 1988.

53. T. Kondo and T. Ohsugi, private communication.

54. J. Kirkby, T. Kondo, S.L. Olsen et al, Proceedings of the Workshop on Experiments, Detectors, and Experimental Areas for the Supercollider, Berkeley, California, p. 388 (1988), eds. R. Donaldson and M.G.D. Gilchriese.

55. T. Ohsugi, H.Ikeda, and T. Kondo, "Radiation Damage Effects on Silicon Detectors in the SSC Environment with L = 10^{33} $cm^{-2}s^{-1}$," Appendix 4 of "Radiation Effects at the SSC," SSC-SR-1035, edited by M.G.D. Gilchriese (1988).

56. Private discussions with industry.

57. V. Radeka and S. Rescia, Nucl. Instrum. and Methods A265, 228 (1988).

58. T. A. Gabriel and W. Schmidt, Nucl. Instrum. and Meth. 134, 271(1976).

59. K. C. Chandler and T. W. Armstrong, ORNL-4744, Oak Ridge National Laboratory (1972).

60. H. W. Bertini, Phys. Rev. 188, 1711(1969).

61. M. B. Emmett, ORNL-4972, Oak Ridge National Laboratory (1975).

62. N. M. Greene et al., ORNL/TM-3706, Oak Ridge National Laboratory (1973).

INTERNAL DISTRIBUTION

1. F. S. Alsmiller
2. R. G. Alsmiller, Jr.
3. B. R. Appleton
4. D. E. Bartine
5. B. L. Bishop
6–10. T. A. Gabriel
11. D. T. Ingersoll
12. J. K. Ingersoll
13. R. A. Lillie
14. F. C. Maienschein
15. RSIC
16. C. Zeigler
17. EPMD Reports Office
18–19. Laboratory Records Department
20. Laboratory Records, ORNL-RC
21. Document Reference Section
22. Central Research Library
23. ORNL Patent Section

EXTERNAL DISTRIBUTION

24. Office of Assistant Manager, for Energy Research and Development, Department of Energy, Oak Ridge Operations, P.O. Box 2001, Oak Ridge, TN 37831
25–34. Office of Scientific and Technical Information, P.O. Box 62, Oak Ridge, Tennessee 37830
35. Argonne National Laboratory, Library Services Dept., 302-CE125, 9700 S. Cass Avenue, Argonne, IL 60439
36. T. W. Armstrong, Science Applications, Inc., PO Box 2807, La Jolla, CA 92038
37. Miguel Awschalom, National Accelerator Laboratory, PO Box 500, Batavia, IL 60510
38. V. S. Barashenkov, Laboratory of Theoretical Physics, Joint Institute for Nuclear Research, Head Post Office, PO Box 79, Moscow, USSR
39. Gerald W. Bennett, Brookhaven National Laboratory, Upton, NY 11973
40. D. Berley, National Science Foundation, Washington, DC 20550
41. Elliott Bloom, Stanford Linear Accelerator Center, PO Box 4349, Stanford, CA 94305
42–46. J. Brau, University of Oregon, Eugene, OR 97403
47. Bruce Brown, Fermi National Accelerator Laboratory, PO Box 500, Batavia, IL 60510
48. David O. Caldwell, Dept. of Physics, University of California, at Santa Barbara, Santa Barbara, CA 93106
49. Stanley B. Curtis, Lawrence Radiation Laboratory, Bldg. 29, Room 213, Berkeley, CA 94720
50. Herbert DeStaebler, Stanford Linear Accelerator Center, Stanford University, Stanford, CA 94305
51. A. DiCiaccio, CERN, Geneva 23, Switzerland
52. J. J. Dorning, Dept. of Nucl. Eng., and Engineering Physics, University of Virginia, Charlottesville, VA 22901
53. R. D. Edge, Physics Department, University of South Carolina, Columbia, SC 29208
54. R. Eisenstein, Department of Physics, University of Illinois, Urbana, IL 61801

55. R. W. Ellsworth, George Mason University, Fairfax, VA 22030
56. Chris Fabjan, CERN, Geneva 23, Switzerland
57. G. Feldman, Stanford Linear Accelerator Center, Stanford University, Stanford, CA 94305
58. W. T. Ford, Experiment 1A-Lab C, Fermi National Accelerator Laboratory, PO Box 500, Batavia, IL 60510
59. E. Fowler, Department of Physics, Purdue University, West Lafayette, IN 47907
60. H. T. Freudenreich, University of Maryland, College Park, MD 20742
61. E. Freytag, Deutsches Elektronen-Synchrotron, DESY, 2 Hamburg Drive, Flottbek, Notkesteig 1, West Germany
62. M. G. D. Gilchriese, SSC Central Design Group, Lawrence Berkeley Laboratory, Berkeley, CA 94720
63. G. T. Gillies, Department of Physics, University of Virginia, Charlottesville, VA 22901
64. G. E. Gladding, University of Illinois, Department of Physics, Urbana, IL 61801
65. K. Goebel, Health Physics Group, CERN, 1211 Geneva 23, Switzerland
66. J. A. Goodman, University of Maryland, College Park, MD 20742
67. M. Goodman, Bell Communication Research, Morristown, NJ 07960
68. D. Groom, SSC Central Design Group, Lawrence Berkeley Laboratory, Berkeley, CA 94720
69. Herman Grunder, Deputy Director, General Sciences, Lawrence Berkeley Laboratory, 1 Cyclotron Rd, Berkeley, CA 94720
70. H. J. Hargis, University of Tennessee, Department of Physics, Knoxville, TN 37919
71. Frenc Hajnal, Health and Safety Laboratory, U.S. Department of Energy, 376 Hudson St, New York, NY 120014
72. R. M. Haralick, Department of Electrical Engineering, University of Washington, Seattle, WA 98195
73. M. Hofert, CERN, 1211 Geneva 23, Switzerland
74. Terrence Jensen, Department of Physics & Astronomy, The University of Rochester, Rochester, NY 14726
75. D. Lal, Tata Institute of Fundamental Research, National Centre of the Government of India, for Nuclear Science & Mathematics, Homi Bhabha Rd, Bombay 5, India
76. Lawrence Livermore Laboratory, Technical Information Department, PO Box 808, Livermore, CA 94550
77. V. Lebedev, Institute of High Energy Physics, Serpukhov, Moscow Region, USSR
78. Library for Nuclear Science, Massachusetts Institute of Technology, at Middleton, Middleton, MA 01949
79. J. LoSecco, Department of Physics, California Institute of Technology, Pasadena, CA 91125
80. J. Marks, Accelerator Fusion Research Division, Lawrence Berkeley Laboratory, 1 Cyclotron Rd, Berkeley, CA 94720
81. A. I. Mincer, University of Maryland, College Park, MD 20742
82. V. S. Narashimham, Tata Institute of Fundamental Research, Bombay 400 005, India
83. W. R. Nelson, Stanford Linear Accelerator Center, Stanford University, PO Box 4349, Stanford, CA 94305

84. T. R. Palfrey, Jr., Department of Physics, Purdue University, West Lafayette, IN 47907
85. Robert Palmer, Brookhaven National Laboratory, Upton, NY 11973
86. C. W. Peck, Department of Physics, California Institute of Technology, Pasadena, CA 91109
87. J. Ranft, Karl-Marx University, Physics Section, Linnestrasse 5,701, Leipzig, East Germany
88. Lincoln Read, Division of High Energy, and Nuclear Physics, Department of Energy, Washington, DC 20545
89. Jim Reidy, University of Mississippi, University, MS 38677
90. C. Rubbia, Lyman Laboratory, Harvard University, Cambridge, MA 02138
91. W. Schmidt, Institute of Experimental Nucl. Phys., University of Karlsruhe, 75 Karlsruhe, West Germany
92. The Secretary, Radiation Group, Lab II, CERN, 1211 Geneva 23, Switzerland
93. Walter Selove, University of Pennsylvania, Department of Physics, Philadelphia, PA 19104
94. B.S.P. Shen, Department of Astronomy, University of Pennsylvania, Philadelphia, PA 19104
95. M. Shupe, Department of Physics, University of Minnesota, Minneapolis, MN 55455
96. Alan Stevens, Physics Department, Brookhaven National Laboratory, Upton, NY 11973
97. G. R. Stevenson, Radiation Protection Group, Lab II, CERN, 1211 Geneva 23, Switzerland
98. L. Sulak, Department of Physics, University of Michigan, Ann Arbor, MI 48109
99. R. F. Taschek, Los Alamos National Laboratory, PO Box 1663, Los Alamos, NM 87544
100. R. Tesch, DESY, Hamburg, Notkesteig 1, West Germany
101. R. H. Thomas, Lawrence Radiation Laboratory, Health Physics Department, Bldg. 72, Berkeley, CA 94720
102. V. D. Toneev, Laboratory of Theoretical Physics, Joint Institute for Nuclear Research, Head Post Office, PO Box 79, Moscow, USSR
103. S. C. Tonwar, University of Maryland, College Park, Md 20742
104. W. Turchinetz, Massachusetts Institute of Technology, R26-411, Cambridge, MA 02139
105. Jim Walker, University of Florida, Gainesville, FL 32611
106. W. J. Willis, CERN, Geneva 23, Switzerland
107. D. Winn, Lyman Laboratory, Harvard University, Cambridge, MA 02138
108. J. Wilczynski, Nuclear Research Center, Karlsruhe, West Germany
109. S. Yellin, Stanford University, Stanford Linear Accelerator Center, PO Box 4349, Stanford, CA 94305
110. G. B. Yodh, University of Maryland, College Park, Md 20742
111. S. Youssef, SCRI, Florida State University, Tallahassee, FL 32306